Testing and Analysis of a Composite Non-Cylindrical Aircraft Fuselage Structure, Part I: Ultimate Design Loads

Adam Przekop,[1] Dawn C. Jegley,[1] Andrew E. Lovejoy,[1] Marshall Rouse[2]
NASA Langley Research Center, Hampton, VA 23681

and

Hsi-Yung T. Wu[3]
The Boeing Company, Huntington Beach, CA 92647

The Environmentally Responsible Aviation Project aimed to develop aircraft technologies enabling significant fuel burn and community noise reductions. Small incremental changes to the conventional metallic alloy-based 'tube and wing' configuration were not sufficient to achieve the desired metrics. One airframe concept identified by the project as having the potential to dramatically improve aircraft performance was a composite-based hybrid wing body configuration. Such a concept, however, presented inherent challenges stemming from, among other factors, the necessity to transfer wing loads through the entire center fuselage section which accommodates a pressurized cabin confined by flat or nearly flat panels. This paper discusses finite element analysis and testing of a large-scale hybrid wing body center section structure developed and constructed to demonstrate that the Pultruded Rod Stitched Efficient Unitized Structure concept can meet these challenging demands of the next generation airframes. Part I of the paper considers the five most critical load conditions, which are internal pressure only and positive and negative g-loads with and without internal pressure. Analysis results are compared with measurements acquired during testing. Performance of the test article is found to be closely aligned with predictions and, consequently, able to support the hybrid wing body design loads in pristine and barely visible impact damage conditions.

I. Introduction

The primary structural concept pursued as an important component of next generation airframe technology under the Environmentally Responsible Aviation (ERA) Project at NASA was the Pultruded Rod Stitched Efficient Unitized Structure (PRSEUS),[1-17] illustrated in Fig. 1. This concept, developed in a collaboration between NASA and The Boeing Company, is intended for application to future transport aircraft with the goal of developing lighter structure so that the aircraft will require less fuel and produce fewer pollutants. The PRSEUS structure is highly integrated, structurally efficient, and has damage-arresting capabilities. In this concept, a stitched carbon-epoxy material system is used. By stitching through the thickness of a dry material system, the labor associated with panel fabrication and assembly can be significantly reduced. When stitching through the thickness of pre-stacked skin, stringers, and frames, the need for mechanical fasteners is almost eliminated. In addition, stitching arrests

[1] Senior Aerospace Research Engineer, Structural Mechanics and Concepts Branch, Mail Stop 190, 8 West Taylor Street, Associate Fellow AIAA.
[2] Senior Aerospace Research Engineer, Structural Testing Branch, Mail Stop 190, 8 West Taylor Street. Senior Member AIAA.
[3] Associate Technical Fellow, Boeing Research and Technology, MC H017-D601, 14900 Bolsa Road.

delamination and improves damage tolerance, allowing for a lighter structure with more gradual failures than traditional composites which do not have through-the-thickness reinforcement.

The PRSEUS concept consists of carbon-epoxy panels fabricated from dry components that are stitched together, after which the resin is infused in an oven while the panel is subjected to vacuum pressure. Skins, flanges, and webs are composed of layers of carbon material that are knitted into multi-ply stacks. A single stack has the thickness of 0.052 in. and comprises seven plies with stacking sequence [+45, −45, 0, 90, 0, −45, +45] and percentage of the 0, 45 and 90-degree fibers equal to 44.9, 42.9, and 12.2, respectively. Several knitted stacks are used to build up the desired thickness and configuration. Stiffener flanges are stitched to the skin using Vectran® thread and no mechanical fasteners are used for joining. To maintain the panel geometry during fabrication, first stiffeners and then the skin are placed in a tool for stitching prior to moving the assembly to a curing tool for consolidation in the oven. The stiffeners running in the S direction in Fig. 1a (stringers) consist of unidirectional carbon fiber rods at the top of the web, which is formed from the stack material and overwraps the rod. The stiffeners in the F direction in Fig. 1a (frames) are foam-filled sandwich structures. The manufacturing process is described in detail in Ref. 6.

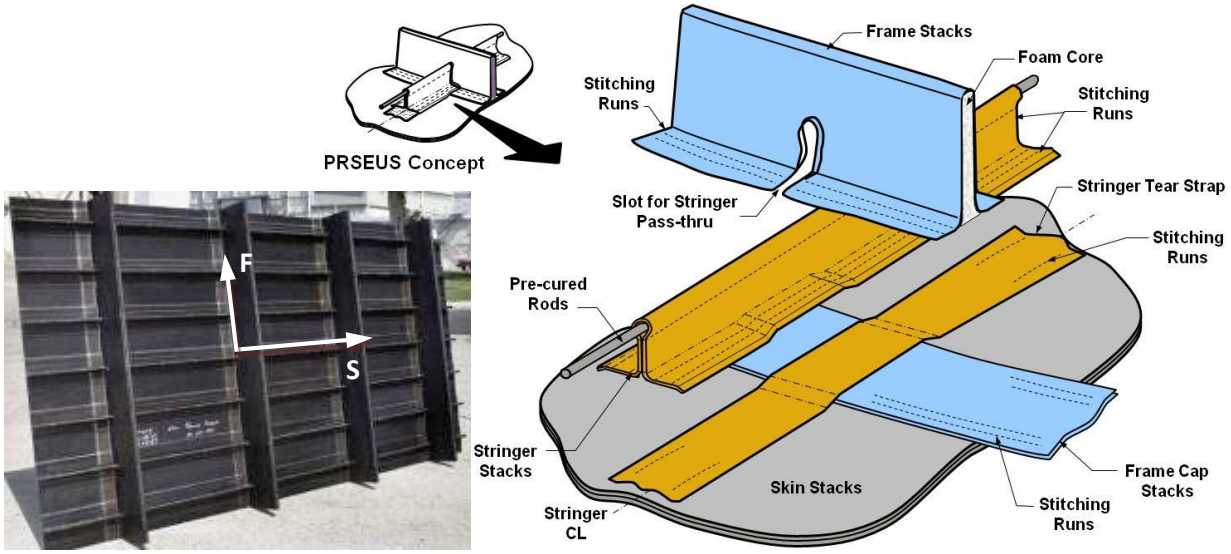

(a) **(b)**

Figure 1. PRSEUS: (a) sample flat panel and (b) general assembly concept.

Numerous test articles utilizing the PRSEUS concept have been built and tested. Typically only individual load conditions such as tension,[9,13] compression[7,9,12] or pressure[8,9,11] were applied as a conventional building-block approach was followed. However, testing under the combined load environment, inherent to the center section of a hybrid wing body (HWB) airframe, has not been conducted prior to the tests described in this paper. As illustrated in Fig. 2, the top center section of a HWB fuselage is required to sustain loads in each of the three primary directions,[15,16] namely stream-wise (Nx), span-wise (Ny), and normal (Nz). Given the specific PRSEUS panel orientation shown in Fig. 2, the wing bending loads are carried primarily by the frame members while the fuselage bending loads are carried primarily by the stringers.

The overall goal of the effort was to demonstrate that the PRSEUS concept can meet the demanding requirements of the next generation airframe technology. A key element of this effort was the recently completed testing performed at the Combined Loads Test System (COLTS) facility[18] located at the NASA Langley Research Center (LaRC). To demonstrate the viability of the PRSEUS concept, the design and fabrication of a large test article was undertaken by the ERA project.[10,14,17] The assembly drawing of the test article is shown in Fig. 3. The test article was representative of an 80%-scale center section of a HWB 410,000 lb. maximum take-off weight aircraft[7] and, therefore, was suitable for structural performance evaluation under a combined loading environment where the multi-axial in-plane loads are

combined with internal pressure loading. The test article was approximately 30 feet in span (in the X direction), 14 feet tall (Z direction), and 7 feet deep (Y direction). The exterior shell and floor comprised 11 PRSEUS panels, and the interior ribs comprised four composite sandwich panels. The 11 PRSEUS panels were: one crown, one floor, one center keel, two side keels (left and right), two upper bulkheads (forward and aft), two lower bulkheads (forward and aft), and two outer ribs (left and right). The crown, floor, center keel, and side keel panels were each stiffened by three equally-spaced frames oriented in the span-wise direction (i.e., along the X-axis in Fig. 3) and the stringers were oriented perpendicular to them (i.e., along the Y-axis). The upper and lower bulkhead panels had their frames oriented in the vertical direction (i.e., along the Z-axis), while their stringers were oriented in the span-wise direction (i.e., along the X-axis). The outer rib panels had their frames oriented in the vertical direction (i.e., along the Z-axis), while their stringers were oriented in the horizontal direction (i.e., along the Y-axis). The four sandwich panels were two upper inner ribs (left and right) and two lower inner ribs (left and right). All of the composite panels were mechanically joined at their edges by metallic fittings and fasteners. The assembled test article is shown in Fig. 4.

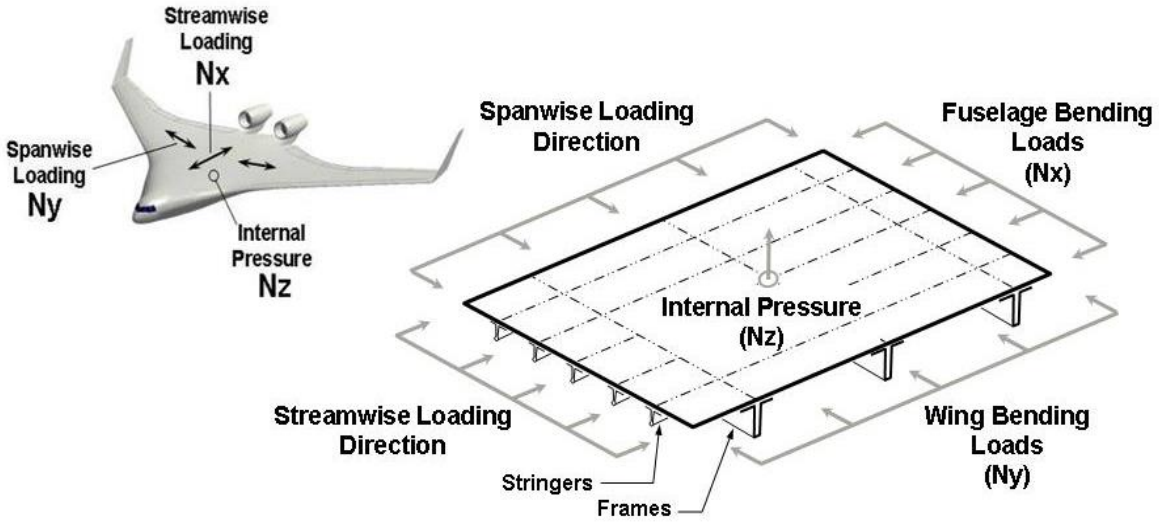

Figure 2. HWB pressure cabin crown panel loading.

The main objective of the analytical component of the activity was to develop a reliable analysis approach applicable to a HWB configuration built using the PRSEUS concept. Initially, due to schedule limitations, a linear finite element analysis (FEA) was used to support the HWB center section test article design effort.[19] Subsequently performed nonlinear analysis, that required considerably longer time, demonstrated that accounting for the geometrically nonlinear effects was warranted for this unconventional configuration.[20] For sufficiently high internal pressure and/or mechanical loads, the small deformation assumption (i.e., less than approximately one-half of the skin thickness) on which the linear analysis is based, is not valid and the nonlinear coupling between in-plane and out-of-plane deformations must be included in the analysis to produce reliable results. As it will be demonstrated later in the paper, for the HWB center section test article, the nonlinear coupling demonstrated itself primarily in two distinct response scenarios. First, local skin buckling is permitted by the PRSEUS design philosophy. The nonlinear analysis was, therefore, needed not only to accurately capture buckling onset but also to predict the large post-buckled deformations. Second, under significant pressure load, or pressure load combined with mechanical loads resulting in tension, the out-of-plane deformations were suppressed, relative to the linear analysis results, by accounting for a significant in-plane tensioning required for the large out-of-plane deformations to occur. Examples of both behaviors are discussed in the results section.

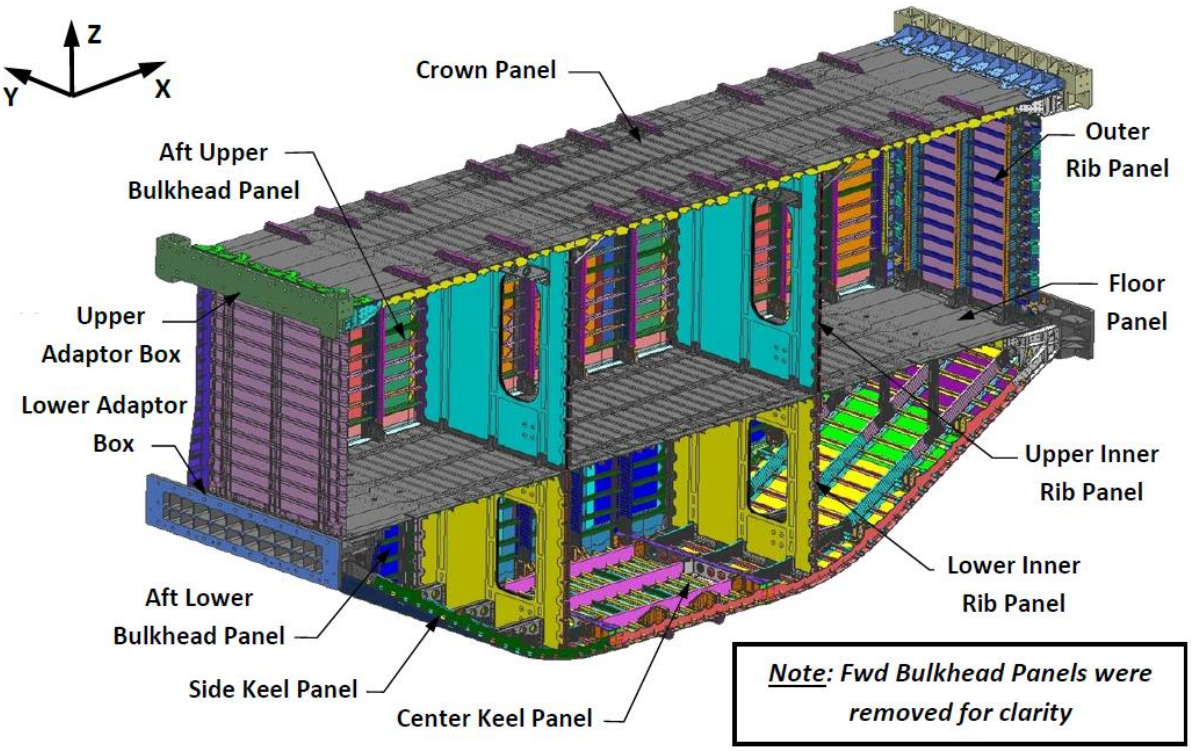

Figure 3. HWB center section test article assembly drawing.

Figure 4. HWB center section test article in a transportation fixture.

II. Predictive Analysis and Testing

This section describes the predictive analysis approach and testing of the HWB center section article. The finite element model (FEM) and analyses are introduced first, followed by the discussion of critical loads and pristine and damaged conditions under which the test article was tested. Finally, the instrumentation used in the test is briefly introduced.

A. Finite Element Model and Analysis

A FEM of the composite panels, metallic fittings, mechanical fasteners, and the COLTS test fixture was developed to support the design and analysis effort. Shell elements were used to represent composite panels and metallic fittings in the HWB center section test article model shown in Fig. 5. The top sections of the frames and the pultruded rods in the panel stringers were represented by beam elements. Connector elements were used to model metallic fasteners. The loading fixtures of the COLTS facility were modeled using a combination of shell and beam elements and are annotated in Fig. 5 to illustrate boundary conditions and test article mechanical load introduction.

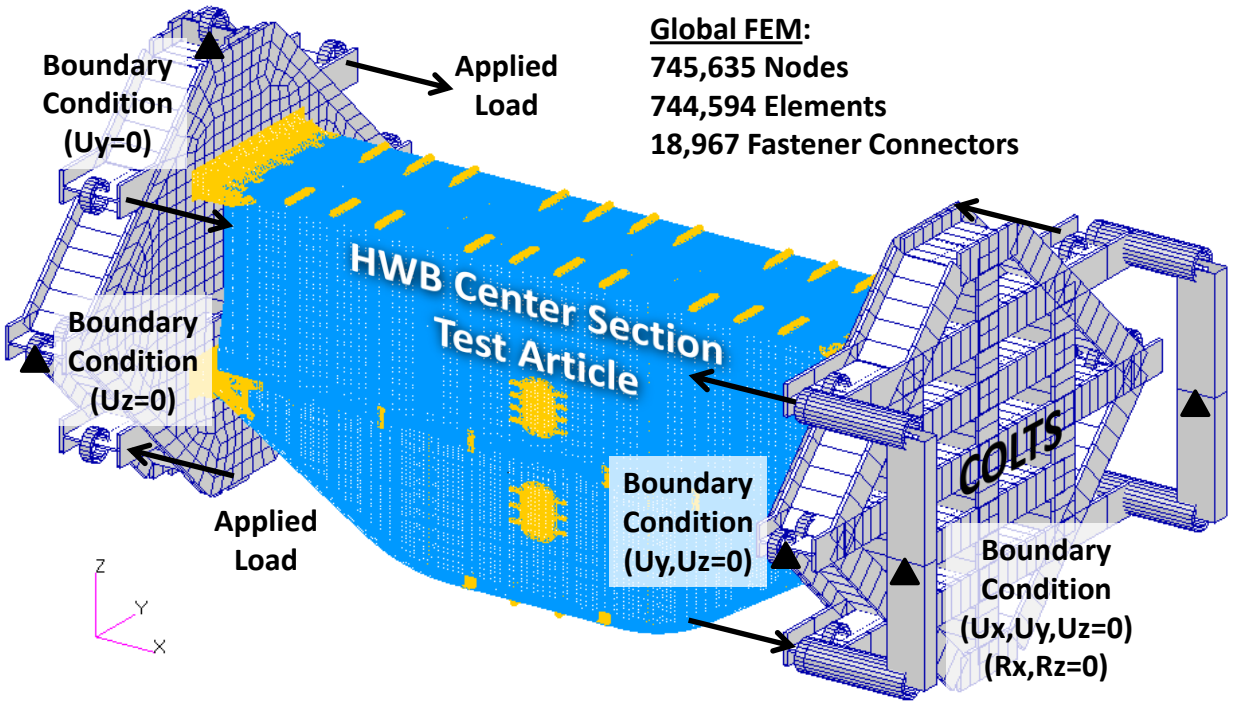

Figure 5. FEM of the test article and the COLTS test fixture.

With the typical element edge size between 0.9 in. and 1.0 in., the FE model contained approximately 4.5 million degrees of freedom. Due to the size of model and the fact that all the fastener elements would need to be removed and redefined again in every re-meshing effort, global mesh convergence studies were not conducted. Local mesh refinements were carried out in the areas of strain concentrations, primarily in the stringers in vicinities of metallic fittings to ensure mesh convergence. In the process of refining the FEM, kinematic constraints were also defined between some of the metallic fittings and underlying sections of composite panels as a simplified and computationally efficient means of reflecting their contact interactions. These kinematic constraints effectively prevented metallic fittings from penetrating composite panels. Together with coarse discretization of the stringers, this interpenetration was initially leading to strain overestimation in the sections of the composite panels near the fittings, particularly in the crown and center keel panels. More details pertaining to this approach are documented in Ref. 21. Otherwise, the modeling practices developed and validated in previous analyses of smaller scale PRSEUS structures[7-9,11-13] were followed. Material properties used in the analysis were the same as those presented in Ref. 20. A nonlinear solver,

known as solution 400, available in the commercial FEA code MSC Nastran,[22] was used. Some of the linear FEA results also presented in this paper for comparison purposes were obtained via solution 101.

B. Critical Loads and Pristine and Damaged Conditions

Previous vehicle level structural sizing studies[1,4,7] identified several critical load cases for the pressurized center section of the HWB. These were 2.5-g wing up-bending and −1.0-g wing down-bending maneuvers, (also known as pitch-up and pitch-down maneuvers), respectively. Additional load cases included the above maneuver loads combined with the cabin pressurization load, i.e., 2.5-g + 1P and −1.0-g + 1P, respectively. Pressure P, determined based on the intended cruise altitude, was assumed to be 9.2 psi in all the HWB structural studies. The above four cases and the pressure-only (also called overpressure) condition of 1.33P, equal to 12.24 psi, were the design limit loads (DLL). When multiplied by a factor of safety of 1.5,[23] a set of five corresponding design ultimate load (DUL) cases was obtained.

The article was initially tested in the pristine condition under the above-mentioned five loading conditions. These loads were applied one at a time as a simple load-and-unload sequence, first to DLL and then to DUL, as shown in Table 1. No known damage was identified after the pristine condition tests were complete. Barely visible impact damage (BVID)[24,25] was introduced to the test article and the above tests were repeated. Since the tests with BVID did not result in any known damage (other than those intentionally inflicted), two out of five load conditions were extended to levels beyond DUL. Namely, the 2.5-g load was extended to 165% DLL (4.125-g) and the 2.5-g + 1P load was extended to 165% DLL of the 2.5-g load component (4.125-g) while the pressure load was kept constant at 150% DLL (13.8 psi). The two "beyond DUL" loads are shown in the far-right column of Table 1. The loading sequence in which the above two loads were applied is shown in Fig. 6. Segment 1 (shown as a black line) in Fig. 6 corresponds to the last BVID DUL test, while segments 2 and 5 (shown as red lines) correspond to the actual "beyond DUL" tests. Segments 3, 4, and 6 (shown in blue) correspond to transitions between the two beyond DUL conditions and the final unloading portion of the test. Since the beyond DUL BVID testing have also not resulted in known damage, a severe damage, referred to also as a discrete source damage (DSD), was inflicted to the crown panel before loading the test article until catastrophic failure was reached.[24,25] The description of the DSD test and analysis, including modification of the FEM, is presented in Part II of this paper.

Table 1. Load cases.

Load Case	DLL	DUL	Beyond DUL
Wing Down-bending	-1.0-g	-1.5-g	N/A
Wing Down-bending with Pressure	-1.0-g + 1P	-1.5-g + 1.5P	N/A
Pressure-only	1.33P	2P	N/A
Wing Up-bending	2.5-g	3.75-g	4.125-g
Wing Up-bending with Pressure	2.5-g + 1P	3.75-g + 1.5P	4.125-g + 1.5P

The applied load vectors, as shown in Fig. 5, correspond to the wing up-bending (positive-g load). Under such a condition, the tops of the platens are pulled together while the bottoms of the platens are pushed apart. Under the wing down-bending condition (negative-g load), the load vectors are reversed relative to those shown in Fig. 5. Better insight into how the loading was applied in the test is provided in Fig.7, which shows the test article installed between the platens connected with the hydraulic actuators in the COLTS facility.

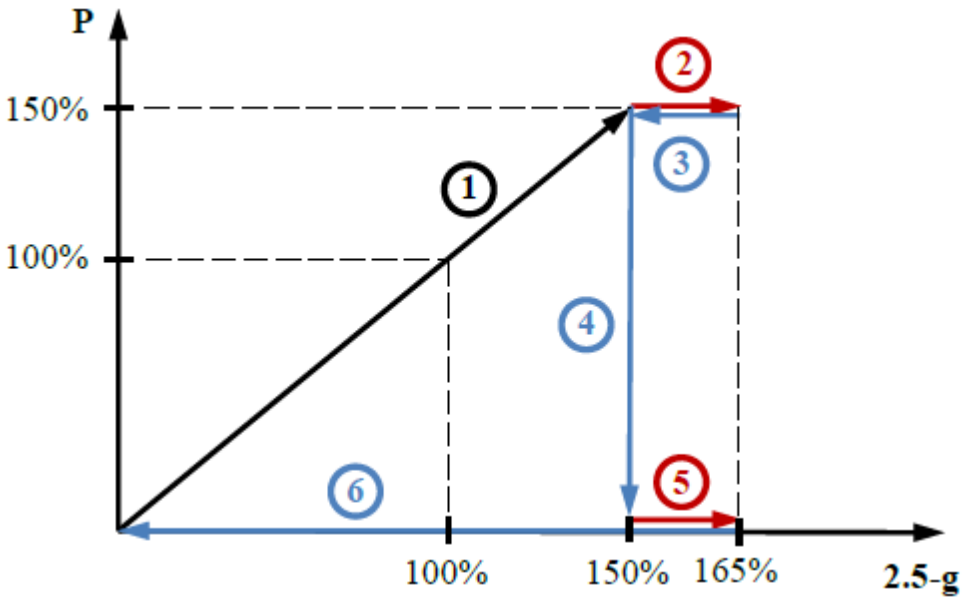

Figure 6. Beyond DUL test sequence.

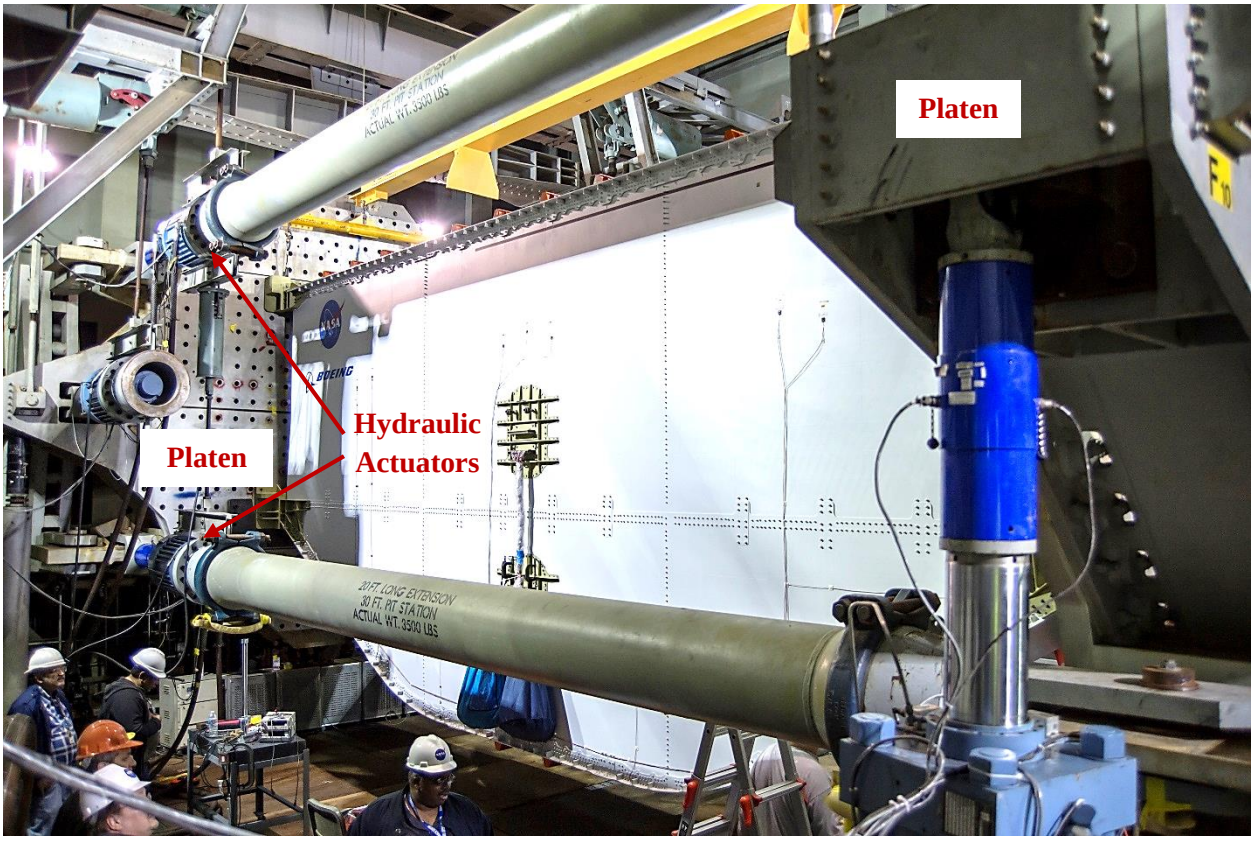

Figure 7. HWB test article installed in the COLTS facility.

C. Test Instrumentation

Five measurement techniques were used during testing and included: (1) video image correlation in three dimensions (VIC-3D),[26] (2) strain gauge measurements, both unidirectional and rosettes, (3) linear variable displacement transducers (LVDTs), (4) fiber-optic strain measurements,[27] and (5) acoustic emission measurements.[28] Still photography, video recordings inside and outside of the test article, and audio recordings were also acquired. The two most extensive and complete sets of measurements, i.e., VIC-3D and strain gauge measurements, are the primary scope of this document.

III. Results

As indicated in section II.B, the tests in pristine and BVID conditions were conducted in two separate series. The FEA, however, was executed only in the pristine condition and no attempt was made to model BVIDs. Comparison of the test results from the pristine and BVID tests confirmed that the BVIDs produced no appreciable effects on the far-field response of the test article.[24,25] Consequently, the comparison of the FEA and test results presented in this section focuses on the far-field or pristine locations. A detailed assessment of BVIDs is offered in a separate report.[29]

While VIC-3D measurements were limited to the outer moldline (OML) surfaces of the crown, bulkhead, and center keel panels, strain gauge data were acquired from both OML and inner moldline (IML) sides of all the panels. Consequently, in the remainder of this section, the out-of-plane nonlinear displacement predictions at DUL are introduced first and compared with available full-field measurements obtained using the VIC-3D system. Deformations of selected panels for which the VIC-3D measurements were not available are illustrated with the FEA results only. Next, discrete strain FEA results are compared with strain gauge measurements at selected characteristic locations on the test article. Displacement plots introduced earlier are used to define general locations where the strain gauge data are compared with FEA predictions (the locations are designated with letters repeated later in the strain figures). Insets showing schematics of a specific strain gauge placement are included in the strain figures. Individual strain gauges are shown in red. If two back-to-back strain gauges are shown in one inset, their colors match the corresponding test strain curves. Strain gauge numbers, consistent with all other test documentation,[21,25] are included in the strain gauge plots. For the unidirectional gauges, their numbers are shown directly in the plot legend. Since including much longer rosette numbers was not practical within the plot legends, their designations are included in figure captions.

Strain gauge test measurements, strains obtained from the linear analysis, and strains obtained from the nonlinear analysis are presented as a function of the applied load. Such plots help to identify sections of the test article which responded in a nonlinear fashion and at what load level the nonlinear effects became apparent and significant. Results for the 2P load case are shown as a function of the pressure load. For the remaining four load cases (−1-g, −1-g + 1P, 2.5-g, and 2.5-g + 1P), the results are shown as a function of the actuator load. For the −1-g + 1P and 2.5-g + 1P load cases, during both analyses and tests, pressure was applied proportionally to the actuator load. Minor departures from this nominal relationship, however, occurred in the test as a result of the limitation of the COLTS pressure control system. The −1-g DLL and DUL levels correspond to actuator loads of 63.6 kips and 95.4 kips, respectively. The 2.5-g DLL and DUL levels correspond to actuator loads of 159 kips and 238.5 kips, respectively. The 2.5-g 165% DLL load corresponds to 262.4 kips actuator loads.

Manufacturing imperfections of the crown panel OML surface resulted in a rework of some sections of the panel. Specifically, repair patches were co-bonded to the skin sections, as shown in Fig. 8 with blue areas. The light blue sections correspond to the single-stack patch thickness and the dark blue sections correspond to the two-stack thickness. The presence of the repair patches was accounted for in the FEM. Local departures from symmetry in the measured and predicted displacement fields shown subsequently in this section stem, at least partially, from the presence of these patches.

The pink features shown in Fig. 8 are the external metallic fittings. The VIC-3D technique is unable to acquire accurate measurements in the vicinities of large surface discontinuities and where shadows obscure the view of the

cameras. These areas are blanked out in the VIC-3D images shown later in this section. These regions include areas with metallic fittings, sensors, and wires.

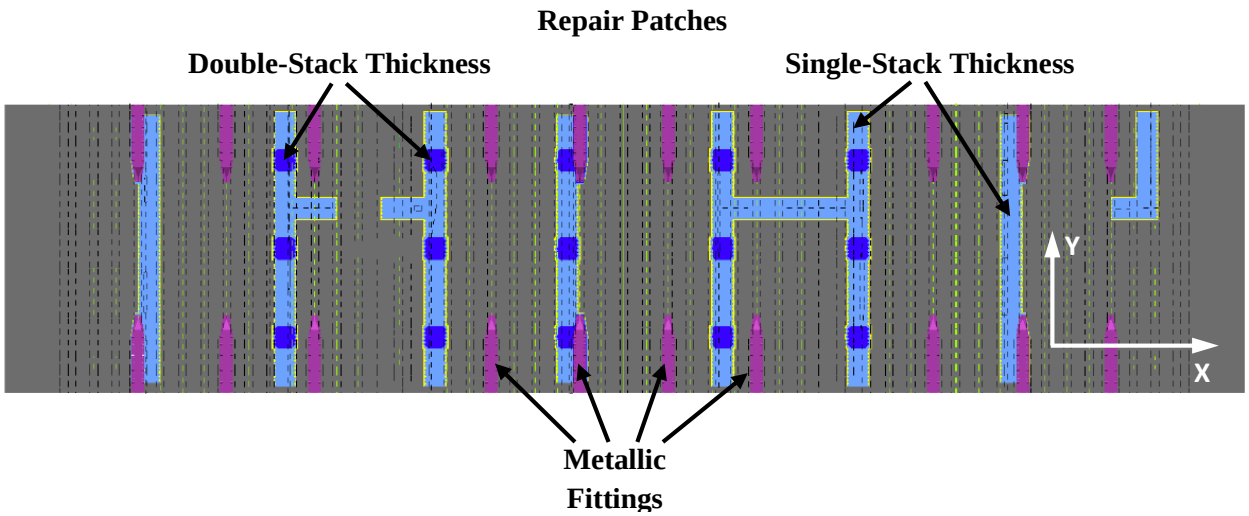

Figure 8. Co-bonded repair patches and external metallic fittings of the crown panel.

Finally, one unintended behavior of the COLTS testing apparatus noted during the tests warrants discussion. Namely, while reviewing displacements and strain recordings from the initial check-out tests, it was concluded that one of the pins in the COLTS loading system was not rotating completely freely. A behavior consistent with the "sticky" pin effect was noticeable in several strain gauge plots as instantaneous small-amplitude strain jumps around otherwise smooth and continuous strain trend developing as the loading was being applied. Despite efforts to resolve the problem, the behavior persisted throughout the entire test effort. Consequently, unless a strain discontinuity is specifically discussed and attributed to another factor, small jumps in strain gauge plots should be regarded as originating from the imperfection of the COLTS load introduction system.

The load cases in this section are discussed in the order in which the BVID tests were conducted. This sequence was determined before the tests based on the predictive nonlinear FEA. The loads were applied beginning with the one resulting in the largest predicted margin-of-safety (MoS)[20] and concluding with the one resulting in the lowest MoS. Such a load application sequence was regarded as a test risk mitigation measure.

A. −1-g Load

Under the −1-g load, the top of the test article was tensioned and the bottom section was compressed. Thus, the most consequential behavior occurred in the center keel panel that experienced extensive local skin buckling under the compressive load, as seen in Fig. 9 showing the out-of-plane deformation under −1-g DUL. While the predicted buckling pattern and associated displacement magnitudes are very similar between the FEA results and test measurements, the location where the alternating outward and inward buckling pattern is perturbed is different. Namely, the FEA analysis predicted the second and the third skin bay (i.e., the skin section confined between consecutive frames and stringers) to the left of the centerline (CL) to buckle in the same direction, while in test the first and the second skin bays to the left of the centerline display this type of behavior (skin bays to the left of the CL are numbered in Fig. 9). A more in-depth discussion of these results is presented later in this section when the strain results are introduced.

Strains in the web of the center frame of the center keel panel just above the frame-stringer intersection are shown in Fig. 10 and correspond to location A in Fig. 9. Compressive strain at DUL is of a moderate level (approximately −0.0035 in./in.) and display nearly linear behavior. The back-to-back center keel skin strains, corresponding to locations B and C in Fig. 9, are shown in Fig. 11 and display a very different behavior. The thin-skin sections between

frames and stringers buckle at a low load of approximately 40 kips actuator load (or 42% of DUL). In the bottom plot of Fig. 11 (location C), the nonlinear solution and test results agree well, while in the top plot (location B), the top gauge prediction matches closely the bottom gauge test measurement and vice versa. Since the frames and stringers of the center keel panel are placed at equal intervals of 24 in. and 6 in., respectively, the skin bay arrangement can be considered periodic within the panel. Each identical skin bay section buckles at nearly identical load and has two stable post-buckled equilibria, deformed inward and outward, as a trivial isotopic straight compressed beam would have. Small manufacturing imperfections, not reflected in the FEM can, therefore, determine which of the two post-buckled deformations is triggered in the test. Similarly, in the FEA, small numerical solver perturbation (e.g., due to the finite precision of computations and/or integration step increments) can be consequential as for which equilibrium is adopted in the numerical solution. Consequently, the comparison of the nonlinear solution and test results is considered good for both locations shown in Fig. 11, while the linear solution clearly lacks the ability to capture the dominant buckling behavior.

The behavior where a buckled skin section of a panel deforms in the direction opposite to the one predicted by the FEA is not unique to the center keel panel nor to the −1-g load case. An additional example of a similar behavior occurring on the crown panel under the 2.5-g load is discussed later in section III.D.

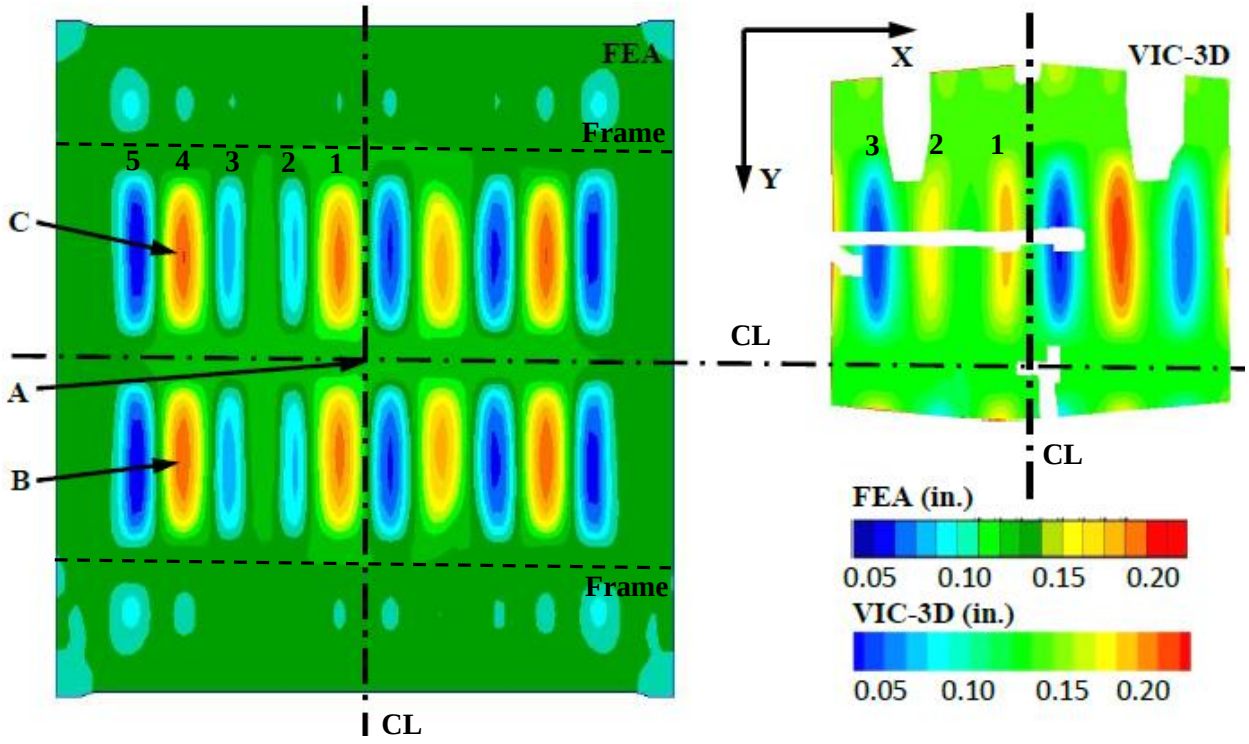

Figure 9. Out-of-plane deformation of the center keel panel under −1-g DUL.

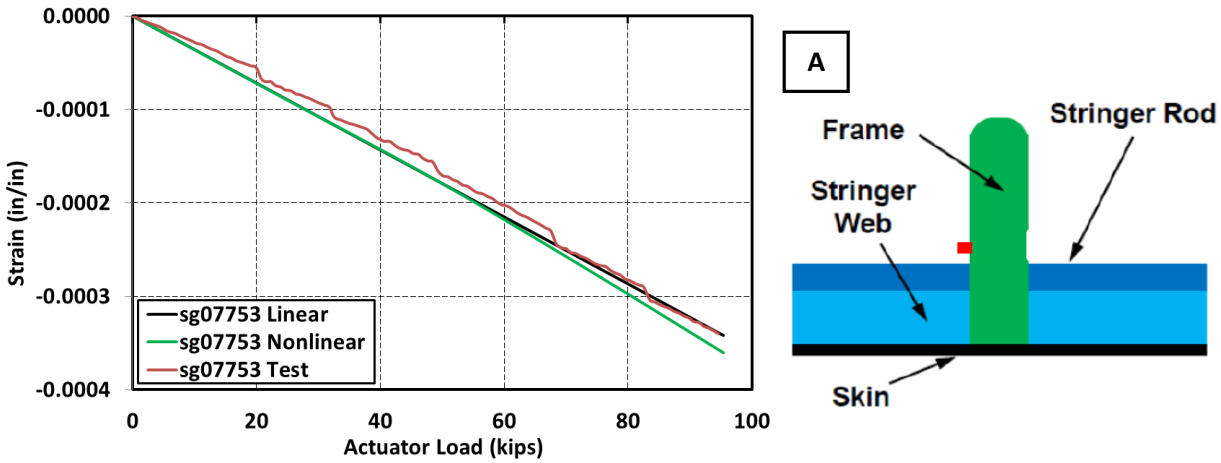

Figure 10. Center keel frame web strains up to −1-g DUL.

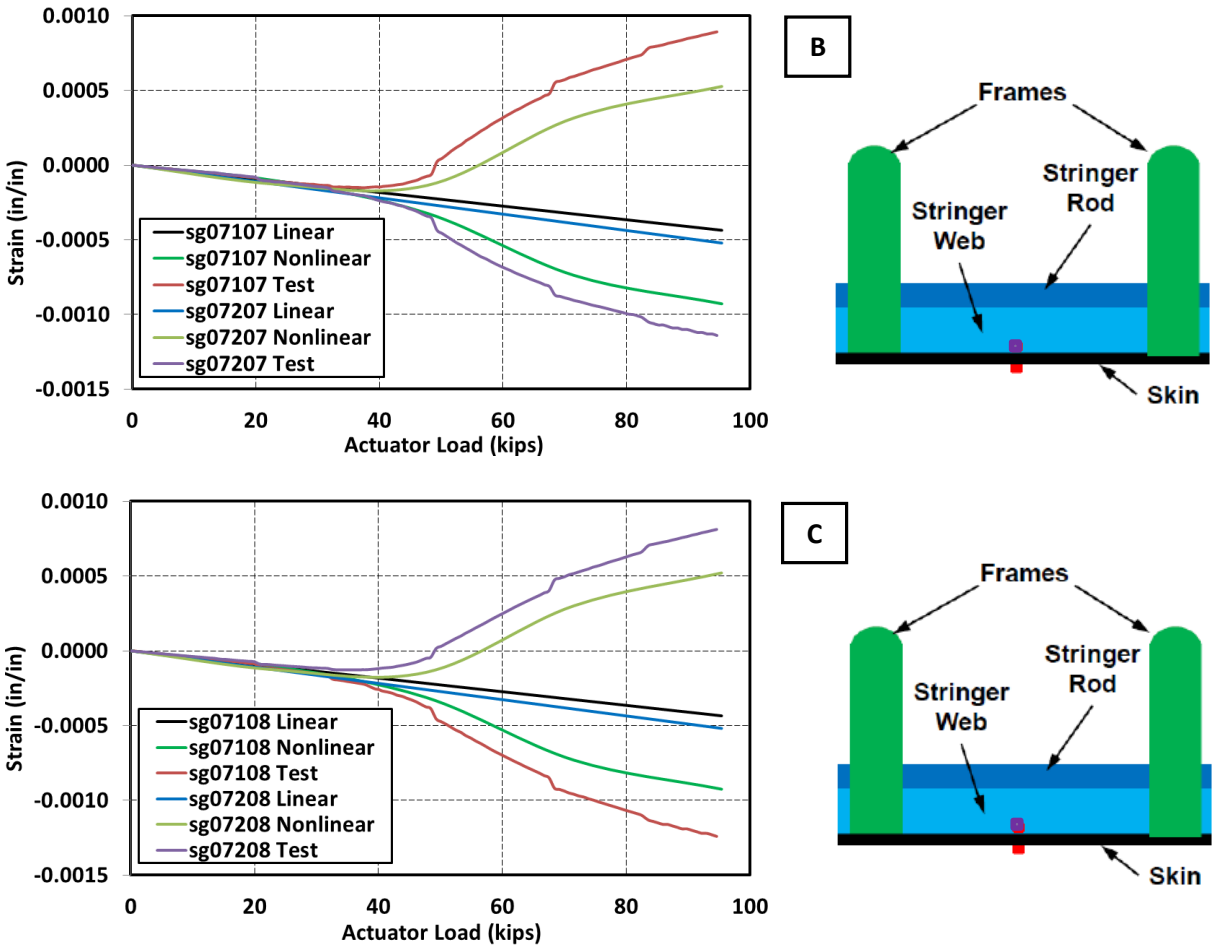

Figure 11. Center keel back-to-back skin strains up to −1-g DUL.

B. −1-g + 1P Load

Under the −1-g + 1P load, the top of the test article was tensioned while the bottom section was compressed by the mechanical loads and the external panels were bowed outward by the pressure load. Thus, the most consequential behavior occurred in the center and side keel panels which experienced the combined effects of mechanical compression and outward bending due to internal pressure. Out-of-plane deformation of the center keel panel at −1-g + 1P DUL is shown in Fig. 12 (the skin bay arrangement is the same as introduced in Fig. 9). Good agreement between the FEA prediction and test measurement is achieved. Relative to the behavior of the center keel panel under −1-g DUL, it is seen that the added pressure load component was able to overcome the effects of the local skin buckling. No alternating inward and outward skin deformation pattern between the stringers and frames is observed. Instead, in addition to the overall outward bowing of the entire panel, the individual skin-bay pillowing is seen.

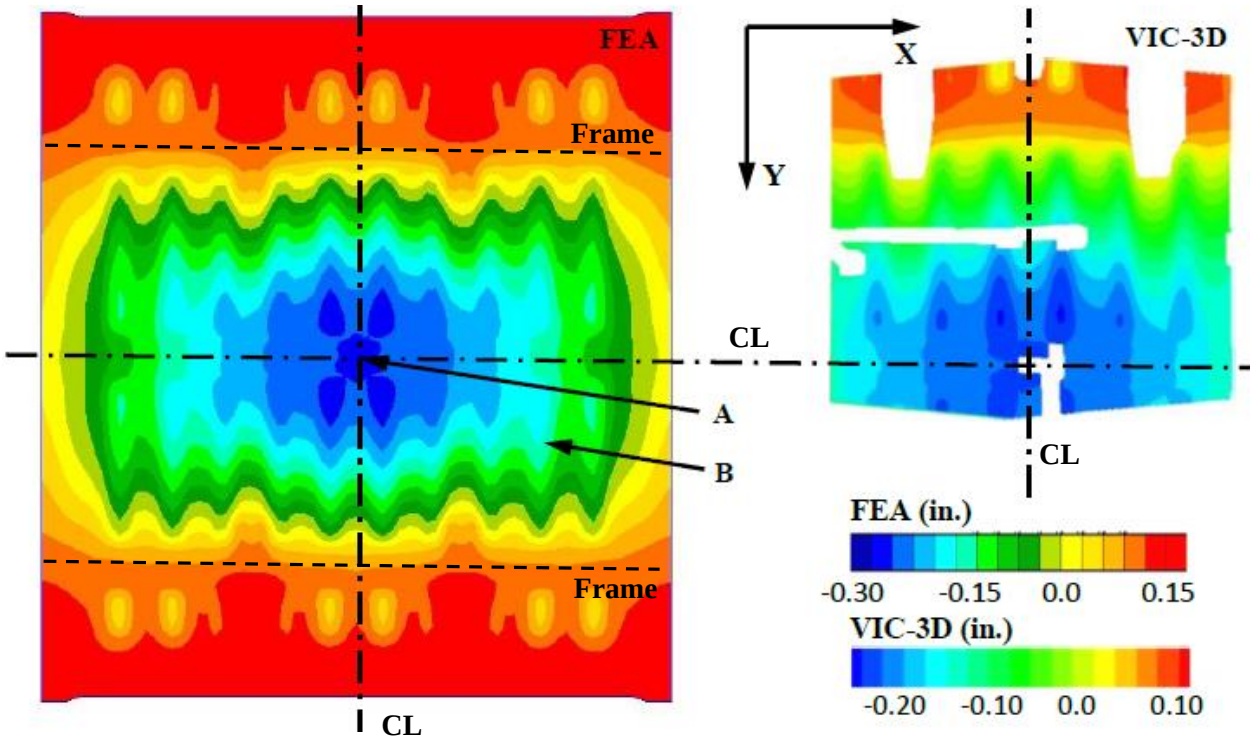

Figure 12. Out-of-plane deformation of the center keel panel under −1-g + 1P DUL.

Strains at the top of the center frame in the center keel panel (location A in Fig. 12) are shown in Fig. 13 and support the described response characteristic. The outward bending of the center keel panel due to the applied pressure stretches the base of the frame and compresses its top. At the same time, mechanical compression of the panel magnifies the pressure-induced compressive strain. Compressive strain reaching −0.002 in./in. at DUL is considered low and shows nearly linear characteristic. While the nearly linear characteristic is accurately captured by the analysis, strain magnitudes are over-predicted by 13% at DUL. To keep the size of the FEM manageable, the sandwich frames were modeled as blades discretized using a single layered shell element across the thickness of the frame, where the foam core was one of the layers, as were the outside composite overwraps. Since this modeling approach did not account for the presence of the overwrap at the top of the frame, rectangular cross-section beam elements were placed there to represent this section of the overwrap. Such a simplification dictated by the computational expediency might have contributed to some loss of fidelity of the analysis at the frame tops.

The center keel panel back-to-back skin strains (location B in Fig. 12) are shown in Fig. 14. The skin strain levels are considered low, as they do not exceed 0.0015 in./in. at DUL, and display a different type of nonlinear characteristic than the skin strains under the previously discussed −1-g load. Unlike the skin behavior under the −1-g load dominated by the alternating inward and outward buckling, under the −1-g + 1P load, the pressure load component forces all skin bays into the outward deformation. As the out-of-plane pressure-induced deformation grows larger, the in-plane stretching of the keel panel skin needs to occur in both X and Y directions. This mechanism, accurately captured by the nonlinear analysis, slows the rate of the out-of-plane deformation growth. Consequently, the test measurements and nonlinear analysis results produce a smaller bending strain component (computed as half of the difference between the OML and IML strains) at DUL when compared to the linear analysis results.

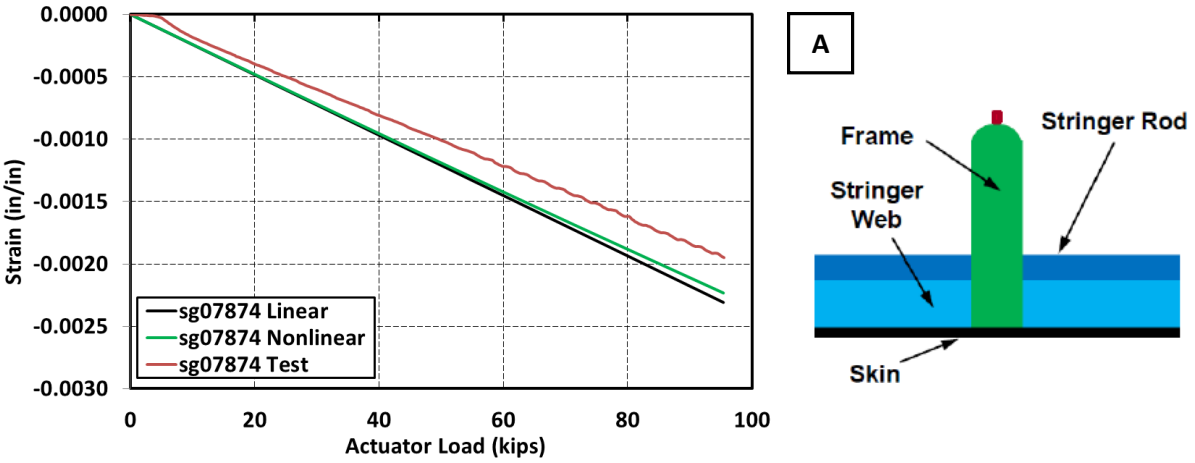

Figure 13. Strains at the top of the center keel panel frame up to −1-g + 1P DUL.

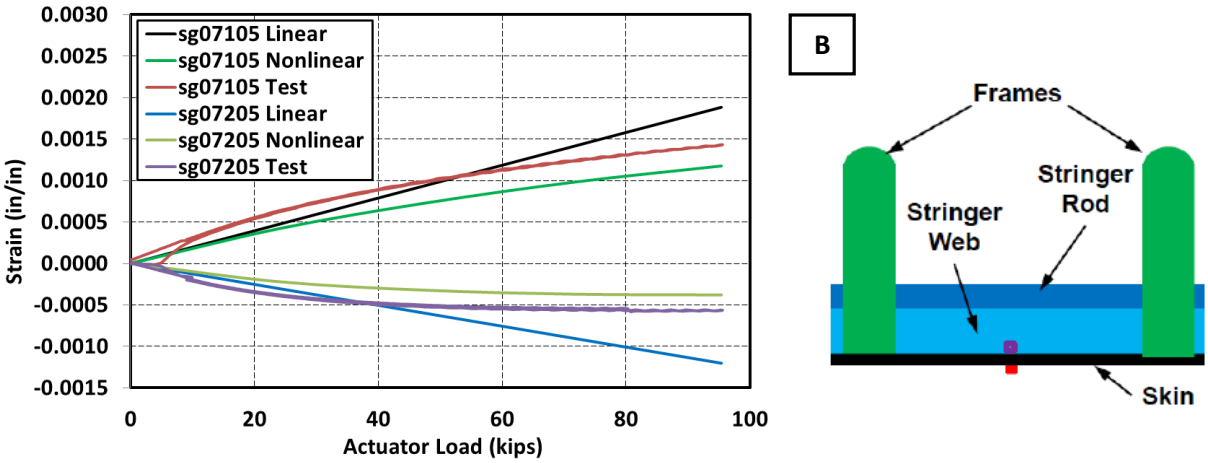

Figure 14. Center keel panel back-to-back skin strains up to −1-g + 1P DUL.

The vertical (Z-axis) deformation component of the side keel panel at −1-g + 1P DUL is shown in Fig. 15. Only the FEA prediction is shown since VIC-3D measurements were not acquired on the side keel panels. Relative to the behavior of the center keel panel under the same load, it is observed, especially in the straight section of the panel away from the inner rib attachment, that the global outward bowing has a more dominant effect when compared to the local skin pillowing. This behavior is primarily driven by the larger size of the side keel panel, and thus the presence of larger unsupported panel sections, which promotes more pronounced development of the global-scale deformation relative to the local pillowing effects.

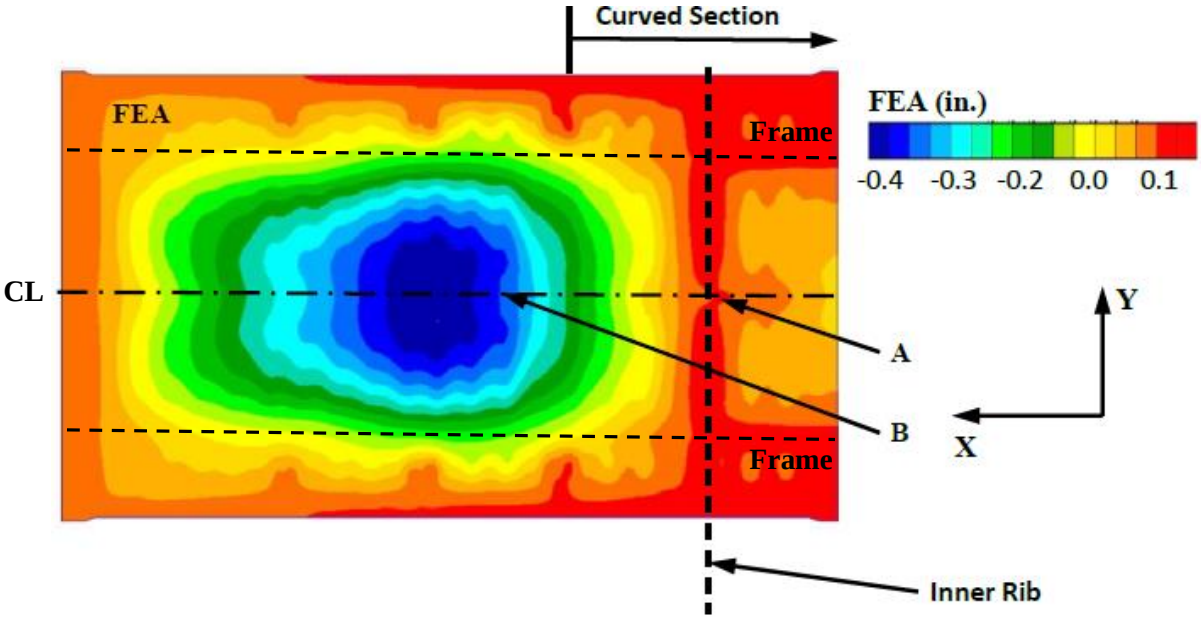

Figure 15. Vertical (Z-axis) deformation component of the side keel panel under −1-g + 1P DUL.

The center frame strains of the side keel panel are shown in Fig. 16 for two different locations. The first location is in the curved section of the frame, closer to the center keel panel and in the proximity of the inner rib (location A in Fig. 15). The second location is in the straight section of the frame, further away from the center keel and the intersection with the inner rib (location B in Fig. 15). A large strain gradient in the center frame of the side keel panel is observed between the two locations. At location B, both mechanical load and pressure load act to compress the top of the frame. At location A, the inner rib reacts the bending moment and the curvature of the panel promotes supporting the normal surface loads more via in-plane tensioning rather than out-of-plane bending. The transition from the tensile to compressive strains is accurately captured by the FEA, however, at DUL the predicted values are overestimating both measured tensile strain of 0.0039 in./in. and compressive strain of −0.0027 in./in. by 15% and 9.8%, respectively.

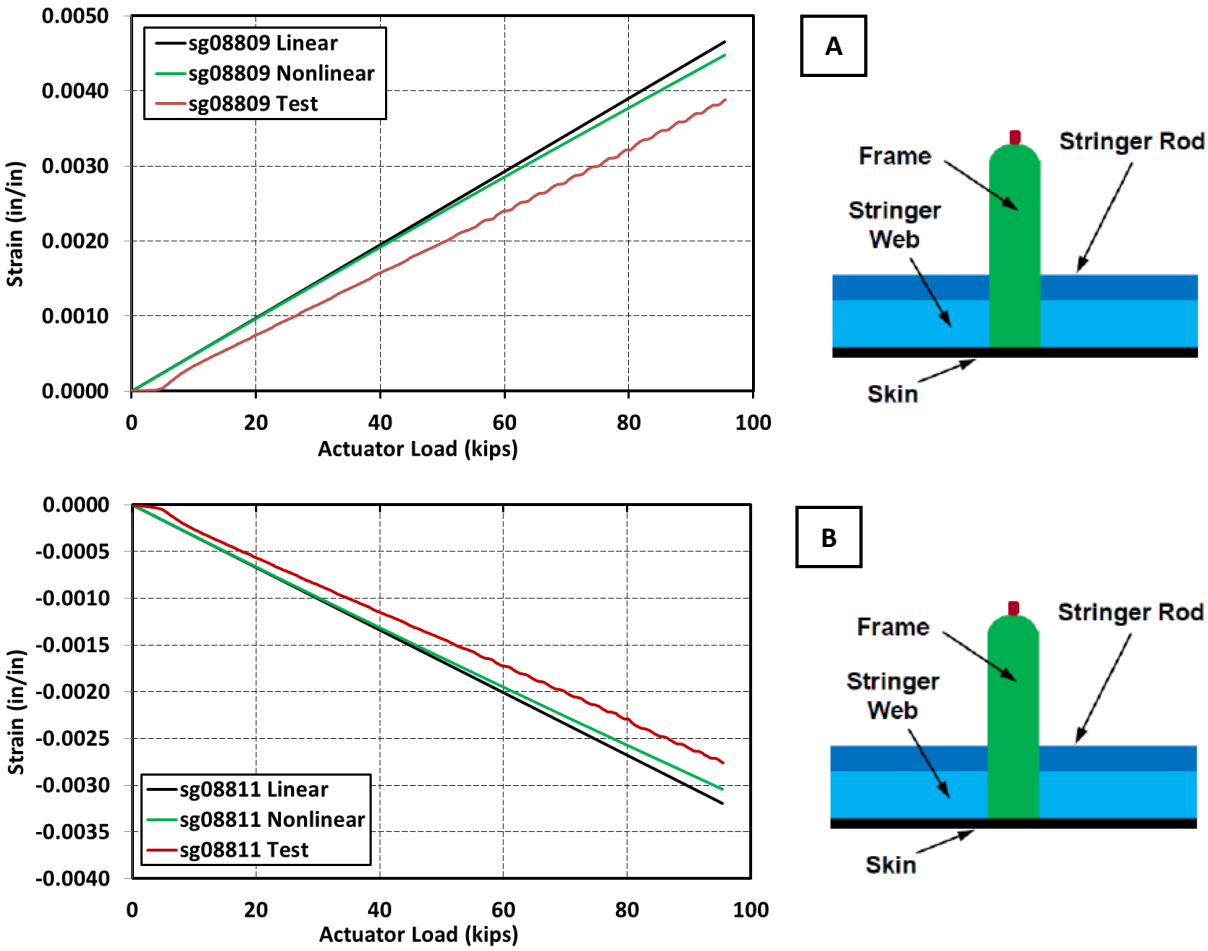

Figure 16. Side keel panel frame top strains up to −1-g + 1P DUL.

C. 2P Load

Under the 2P load external panels bowed outward. Out-of-plane deformations of the upper bulkhead panel at 2P are presented in Fig. 17. The upper bulkhead panel is chosen for the discussion of the 2P load case since this panel features the largest unsupported sections among all the test article panels (approximately 10 ft. by 7.7 ft. in the center section and 8.7 ft. by 7.7 ft. in the side sections), thus the pressure effects are most pronounced in this panel. As shown in Fig. 17, the response of the structure is dominated by the global-level outward deformations where attachments to the adjacent panels, both external and internal, act as panel edge restraints. In addition, local outward deformations associated with individual skin bays are visible as scalloping contours with spacing coinciding with distances between the frames and stringers. At 2P, the predictive FEA overestimated the out-of-plane deformation at point C of Fig. 17 by 16%.

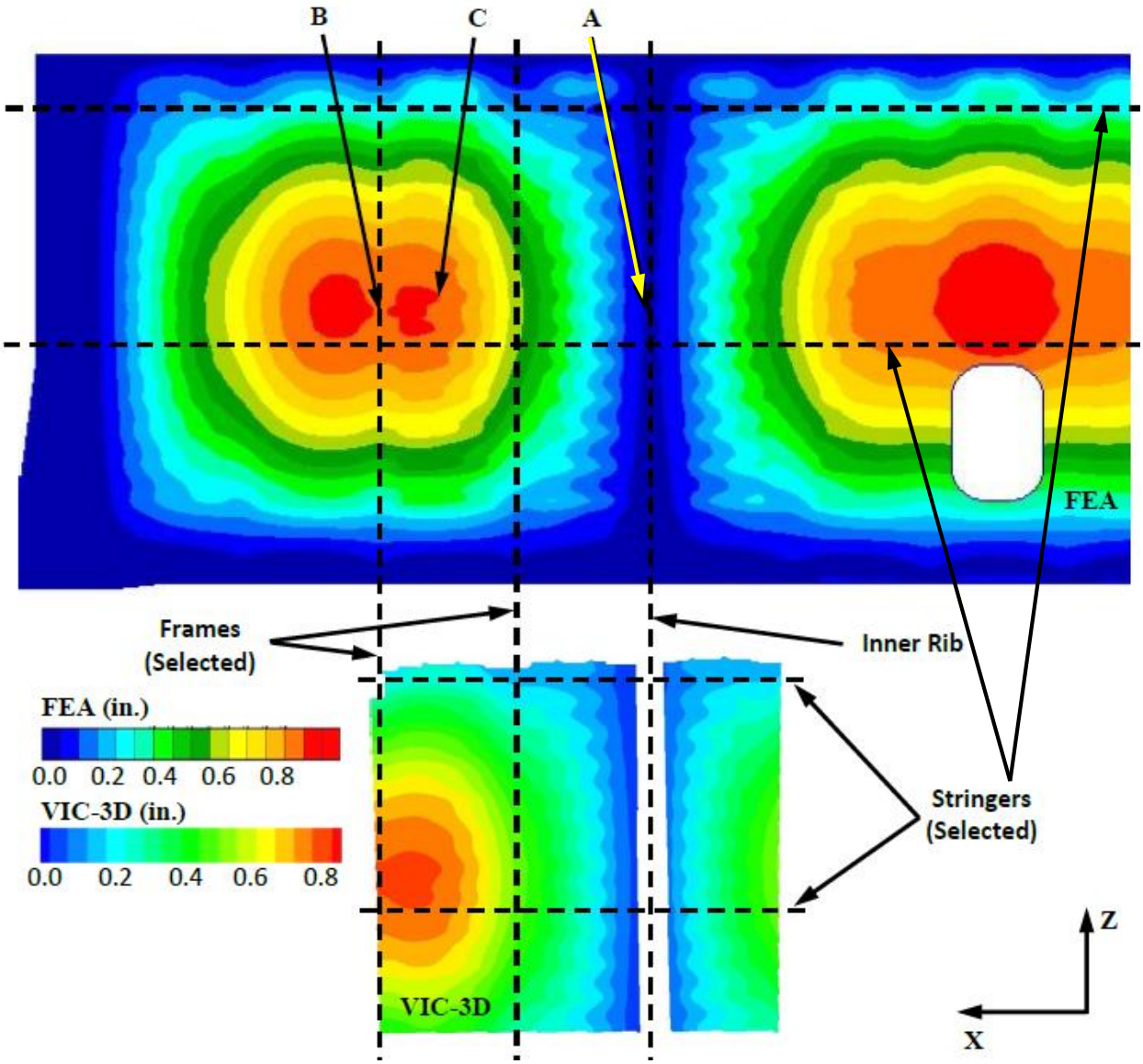

Figure 17. Out-of-plane deformation of the upper bulkhead panel under 2P.

Strains at the top of a stringer (location A in Fig. 17) are shown in Fig. 18, and at the top of a frame (location B in Fig. 17) are shown in Fig. 19. Both display only slightly nonlinear behavior. The strain magnitudes are considered moderately high as the stringer top strain reaches 0.0050 in./in. in tension and the frame top strain exceeds 0.0040 in./in. in compression at the DUL. The FEA predictions at DUL overestimate both measured tensile and compressive strains by 19% and 14%, respectively. While the simplified modeling of the frame tops was discussed in section III.A, a similar discussion is warranted here for the stringer. Again, motivated by keeping the size of the FEM manageable, the stringer tops were modeled as beam elements representing the pultruded rods and were connected to the top of the stringer web modeled as a blade discretized with shell elements. Thus, the overwrap of the pultruded rod was not modeled. This simplification is, at least in part, likely responsible for some of the discrepancies observed between the FEA results and test measurements at the stringer tops.

The upper bulkhead back-to-back skin strains (location C in Fig. 17) display strongly nonlinear behavior, as shown in Fig. 20. The test strains at DUL reach approximately 0.0020 in./in. in tension on the OML surface. The strains predicted by nonlinear FEA and measured in test agree very well (within 1.7% and 4.0% at DUL on the OML and IML surfaces, respectively). The nonlinear behavior seen in Fig. 20 is typical for thin-walled structures subjected to loads in the normal direction. Namely, when large out-of-plane deformations occur, the panel undergoes in-plane stretching. This in-plane tensioning suppresses the out-of-plane deformation growth, which is a factor that is not included in the linear analysis approach. To advance this argument, note that the average of the OML and IML strains, corresponding to the in-plane strain component, is approximately 0.0016 in./in. at DUL for all three results shown in Fig. 20. At the same time, the bending component, i.e., the difference between the in-plane and OML or IML results, is approximately ±0.0005 in./in. for the nonlinear analysis and test, while approximately ±0.0018 in./in. for the linear solution. It is, thus, concluded that not accounting for the afore-mentioned nonlinear coupling results in a large overestimation of the bending strains, as the out-of-plane deformation magnitude is over-predicted as a result of not accounting for the in-plane stretching that needs to accompany large out-of-plane deformations.

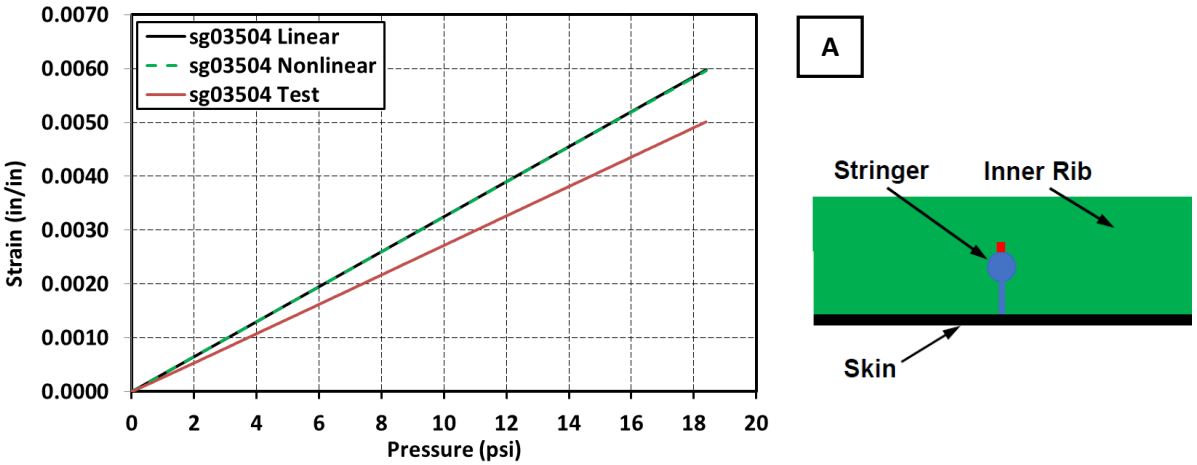

Figure 18. Strains at the top of the upper bulkhead panel stringer up to 2P.

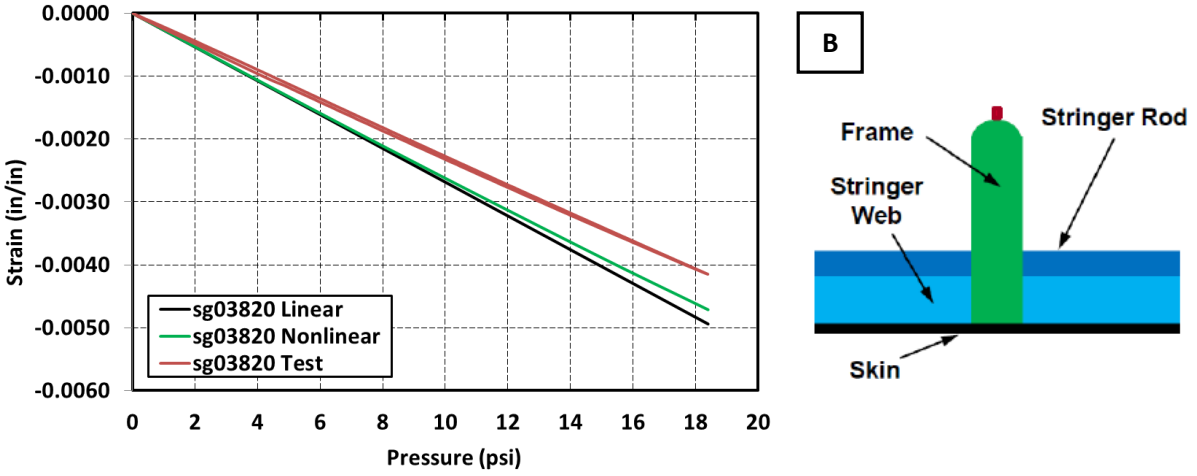

Figure 19. Strains at the top of the upper bulkhead panel frame up to 2P.

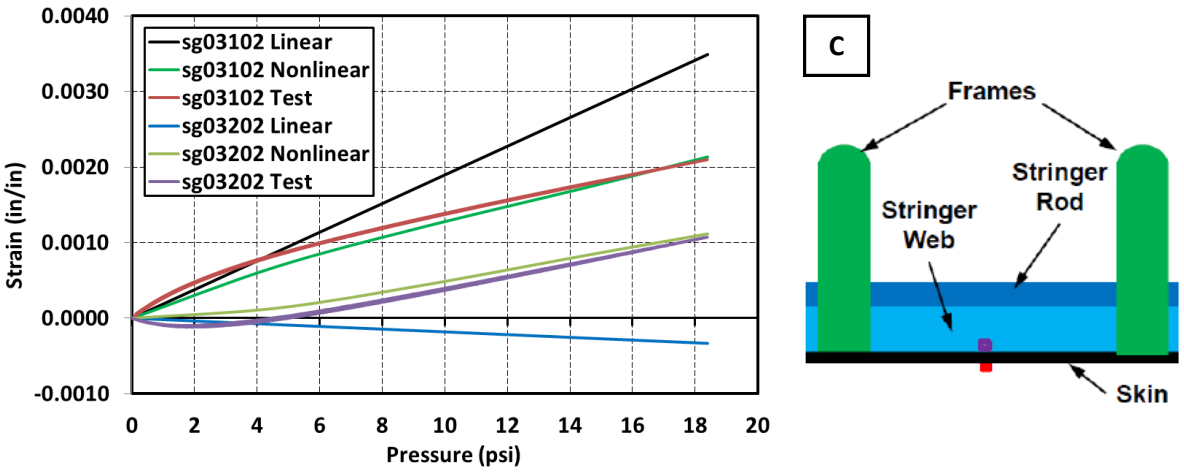

Figure 20. Upper bulkhead panel back-to-back skin strains up to 2P.

D. 2.5-g Load

Under the 2.5-g load, the top of the test article was compressed and the bottom tensioned by the mechanical loads. Thus, the most consequential behavior occurred in the crown panel which experienced extensive localized skin buckling. The crown panel out-of-plane deformation under 2.5-g DUL is presented in Fig. 21. Since the 2.5-g DUL test was conducted twice, once for the pristine and once for the BVID conditions, both test results are included in Fig. 21 to highlight certain features associated with testing and nonlinear analysis of structures with multiple buckling equilibria and periodic construction.

As shown in Fig. 21, the out-of-plane deformation of the crown panel under the 2.5-g load is dominated by the skin buckling which extends almost the entire span of the panel. However, different buckling patterns were obtained in the pristine and BVID tests. Since BVIDs were not applied to the crown panel and no appreciable effects of BVIDs were noted elsewhere in the far-field response, it is concluded that the uniqueness of the deformation field for structures with multiple stable equilibria in their periodic features cannot be guaranteed. It is likely that a particular buckling pattern obtained in each test was triggered by otherwise globally insignificant factors such as small manufacturing imperfections, scatter in the applied load path or minor residual stresses from the previous tests and/or servicing of the test article between the tests.

The lack of uniqueness of the deformation field was not limited to test measurements only. Several nonlinear FEAs were executed with slight changes to solver parameters, such as, e.g., the integration step increment, and also resulted in distinct buckling patterns (not shown here for brevity). None of the measured and predicted patterns, however, matched exactly. Nevertheless, the comparison of the measured and predicted displacement results is considered good, as the characteristic buckling behavior was captured and the displacement magnitudes matched within 14%.

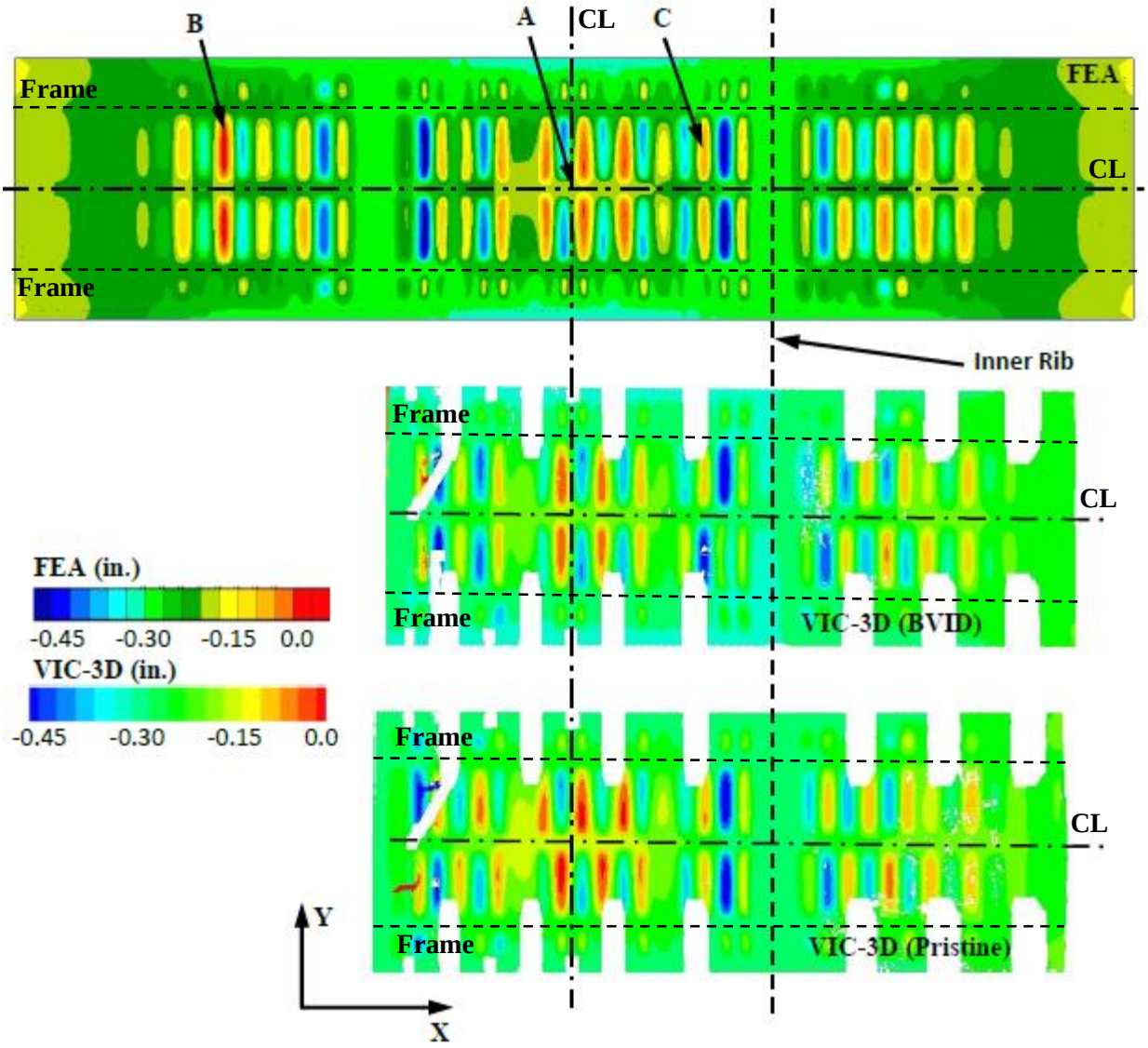

Figure 21. Out-of-plane deformation of the crown panel under 2.5-g DUL.

The crown panel strains at the top of the center frame (location A in Fig. 21) up to 2.5-g 165% DLL are shown in Fig. 22 where a slightly nonlinear characteristic of the frame compressive strain is identified. The test strains slightly exceed the nonlinear FEA prediction and reach approximately −0.0036 in./in. at 150% DLL (or DUL) and −0.0040 in./in. at 165% DLL (i.e., 110% DUL). A slight discontinuity in the test strain curve seen in Fig. 22 around the DUL of 238.5 kips actuator load is due to the fact that the test results for the 2.5-g load are compiled as a sum of the 2.5-g DUL BVID test (up to 238.5 kips) and segment 5 of the "beyond DUL" BVID test presented in Fig. 6 (from 238.5 kips to 262.4 kips actuator load). Similar discontinuities at 238.5 kips actuator load can also be observed later in this section in other strain plots.

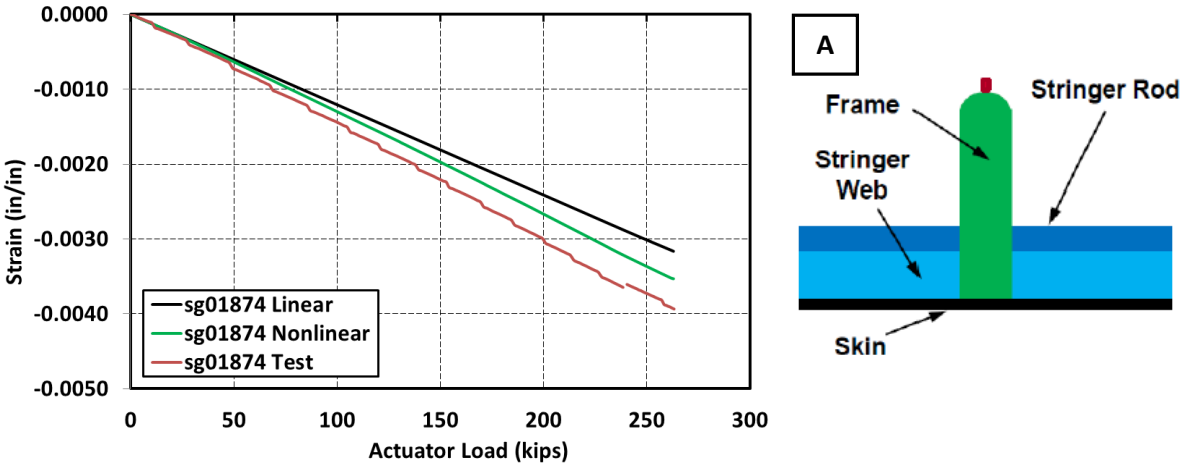

Figure 22. Strains at the top of the crown panel frame up to 2.5-g 165% DLL.

The crown panel IML-side minimum principal skin strains in the side section of the panel near the aft frame flange (location B in Fig. 21) are presented in Fig. 23. A strain gauge rosette was used at this location since the nonlinear FEA predicted appreciable shear strain contribution due to the proximity of the stringer-frame intersection and the metallic fitting used to attach the upper bulkhead to the crown panel (the second fitting from the left in Fig. 8). The back-to-back strains at the mid-bay in the center section of the panel (location C in Fig. 21) are presented in Fig. 24. The unidirectional strain gauges were installed there as the span-wise strains were predicted by the FEA to dominate the response in the middle of the skin bays, i.e., away from frames, stringers, and metallic fittings. Both figures indicate that the crown panel skin buckling occurred early in the loading sequence. For the center section of the crown panel (location C in Fig. 21) where the skin comprises the single stack (0.052 in.), buckling occurred around 30 kips actuator load. For the two stack-thick skin in the side section of the crown panel (location B in Fig. 21), the buckling load was higher, at approximately 60 kips actuator load. It is seen in Fig. 23 that once the skin buckling occurred around 60 kips, the compressive strains began to grow much faster than those predicted by the linear analysis. While the linear analysis predicted approximately −0.0033 in./in. at 165% DLL, the measured strains were close to −0.0063 in./in., that is nearly double the linear FEA prediction. The nonlinear analysis accurately captured the buckling load and the post-buckled behavior by closely predicting both strain characteristic and values (strain magnitude under-predicted by 8.2% at 165% DLL). A good comparison between the test and the nonlinear FEA results was also observed for the back-to-back skin strain results shown in Fig. 24 (maximum and minimum strains at 165% DLL show 12% and 3.2% difference, respectively). Since the IML- and OML-measured strains in Fig. 24 are of similar magnitude, but with opposite signs, it is concluded that the in-plane strain component of the response in the mid-bay skin location was close to zero and the bending strain component of order of ±0.003 in./in. was dominating the response. This behavior is consistent with a strongly developed post-buckled regime that is shown in Fig. 21 to dominate nearly the entire crown panel surface.

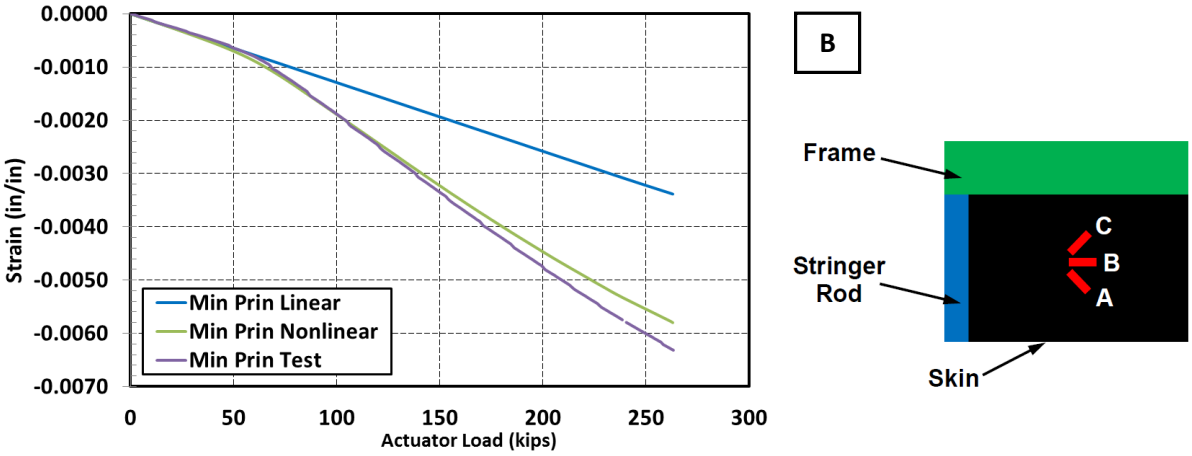

Figure 23. Minimum principal strains in the crown panel skin up to 2.5-g 165% DLL (sg01290A/sg01291B/sg01292C).

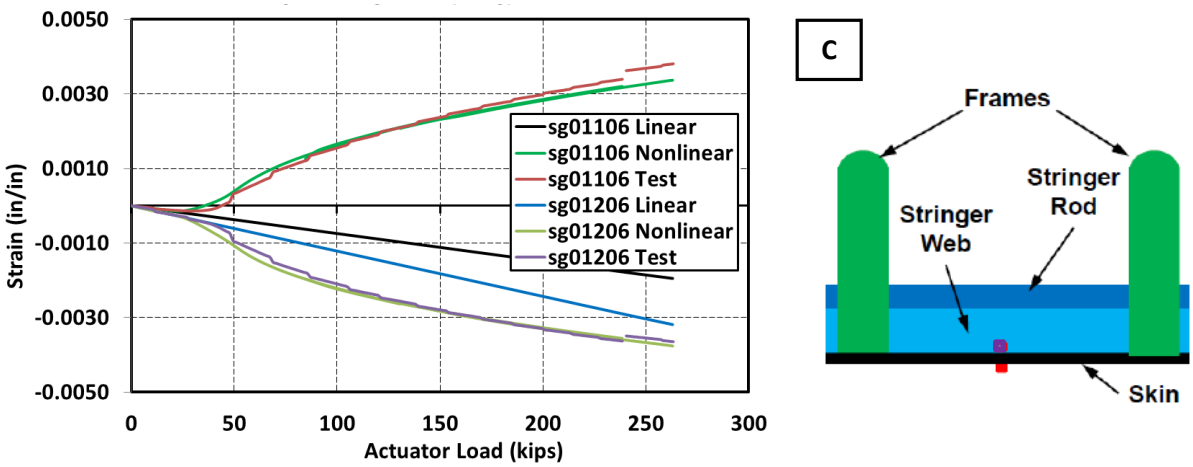

Figure 24. Crown panel skin back-to-back strains up to 2.5-g 165% DLL.

The out-of-plane deformation of the upper bulkhead panel at 2.5-g DUL is shown in Fig. 25. It is seen that the upper bulkhead transferred significant span-wise compressive loads in its top section attached to the crown panel and significantly lower loads at the bottom of the panel (near the neutral bending axis). Similar to the skin sections of the crown panel, these loads produce large out-of-plane skin deformations occurring due to buckling. However, the typical buckling pattern near the top of the upper bulkhead panel (e.g., in the proximity of location A in Fig. 25) is different from that of the crown panel. The buckled skin sections of the crown panel display one semi-sine-like shape per individual skin bay between the consecutive stringers and frames. In the upper bulkhead panel, most of the skin bays display three to four semi-sine-like shapes that are additionally skewed relative to the frame-stringer orthogonal grid. These types of buckling shapes can be explained by the fact that the span-wise edge of each individual skin bay in the bulkhead (24 in. between consecutive frames) is longer than that in the crown panel (6 in. between consecutive stringers). Also, in the upper bulkhead panel, the top edge of the each skin bay is compressed more than the bottom edge of the same skin bay due to the two edges being located at a different distance from the neutral bending axis of the entire test article. This compressive load variation translates into a shear load component resulting in the skewed buckling shapes. Similar to the more regular buckling pattern observed in the crown panel, the skewed buckling shapes are also susceptible to adopting different stable equilibria (additional upper bulkhead deformation plots

demonstrating this observation are not shown for brevity). Also similar to the crown panel results, the comparison of the measurements and predictions is considered good, as the characteristic behavior and displacement magnitudes match closely.

The skin strains in the top section of the upper bulkhead, adjacent to the crown panel and undergoing significant compression, also exhibited strongly nonlinear characteristics due to buckling. The principal skin strains just below the crown-to-bulkhead panel attachment are shown in Fig. 26. Similar to the crown panel skin strains discussed earlier in this section, the minimum principal strain dominating the response grows more rapidly above the buckling load than the linear solution. The loads under which the upper bulkhead skin buckles are, however, generally higher than those discussed previously for the crown panel. This result is supported by the fact that the crown panel skin is located at the furthest distance from the neutral bending axis of the entire test article and the top section of the upper bulkhead operates at a distance closer to the afore-mentioned neutral bending axis. Again, overall good agreement is found between the test results and the FEA predictions (the predicted magnitude of the minimum principal strain is lower by 0.19% than the measured value).

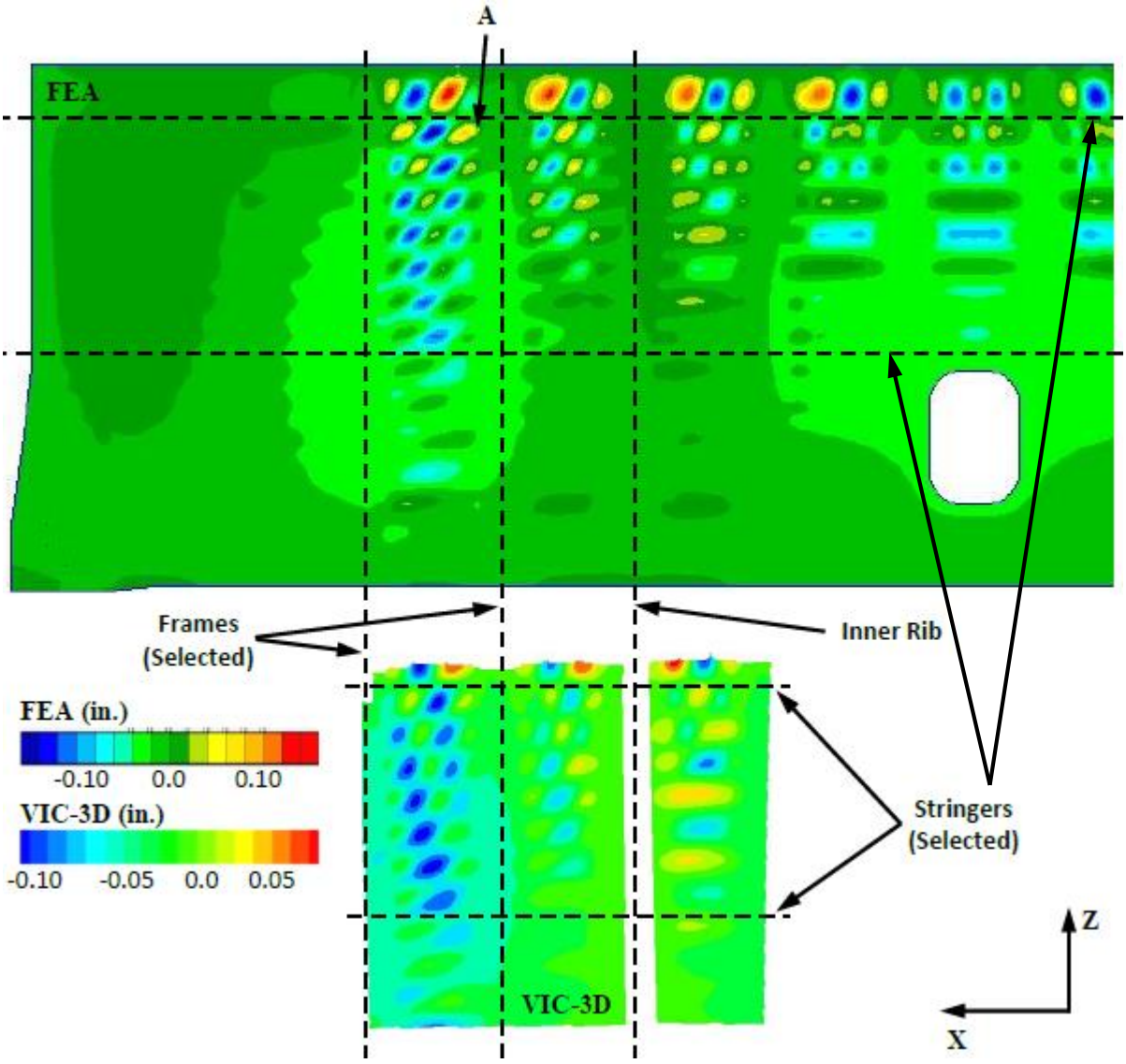

Figure 25. Out-of-plane deformation of the upper bulkhead panel under 2.5-g DUL.

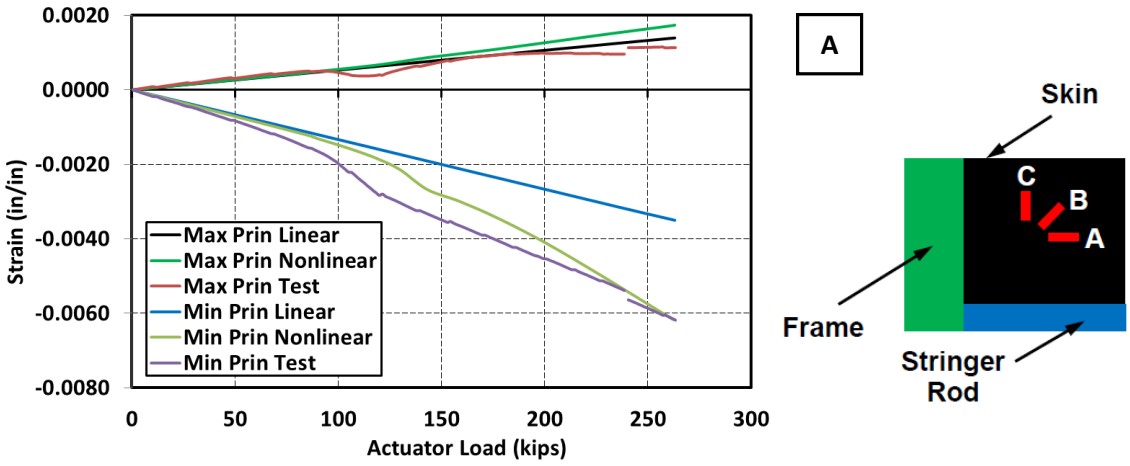

Figure 26. Principal strains in the aft upper bulkhead panel skin up to 2.5-g 165% DLL (sg03111A/sg03112B/sg03113C).

E. 2.5-g + 1P Load

Under the 2.5-g + 1P load, the top of the test article was compressed and the bottom tensioned by the mechanical loads and the external panels were bowed outward by the pressure load. The crown panel out-of-plane deformation under 2.5-g DUL is presented in Fig. 27. All the skin bays in the center section of the crown panel (except for one covered by a span-wise section of the repair patch shown in Fig. 8) are pushed outward by the pressure loading. The outward skin deformation dominates the response at DUL even though initially, when the load was being applied to the test article, some of the center section skin bays buckled inward. This behavior took place because only a low level of mechanical loading was needed to buckle individual skin bays, as documented in section III.D. However, as the load application progressed and the pressure load became larger, the skin surface pressure forces were able to snap the skin bays to the outward position. This was, however, not the case for some of the skin bays in the side sections of the panel, where the skin has a larger thickness. Once such a thicker skin bay buckled due to the mechanical portion of the load, further pressure increase was insufficient to force the inwardly buckled skin section into the alternate outward equilibrium. While the above-described behavior cannot be conclusively discerned from the single crown panel image at DUL, a review of an animation assembled from all the acquired VIC-3D images as the load was increased resulted in the above-described observation. In general, the pressure component of the 2.5-g + 1P load can be regarded as a factor removing some of the uncertainty associated with the out-of-plane displacement results described in section III.D pertaining to the 2.5-g load condition. For example, no differences in the crown panel deformation patterns between the pristine and the BVID tests were observed. Similarly, numerical simulations conducted with different integration steps also yielded identical results. Overall, a good qualitative agreement is found between the nonlinear FEA and test measurements (the FEA over-predicted the out-of-plane deformation magnitude by 17%).

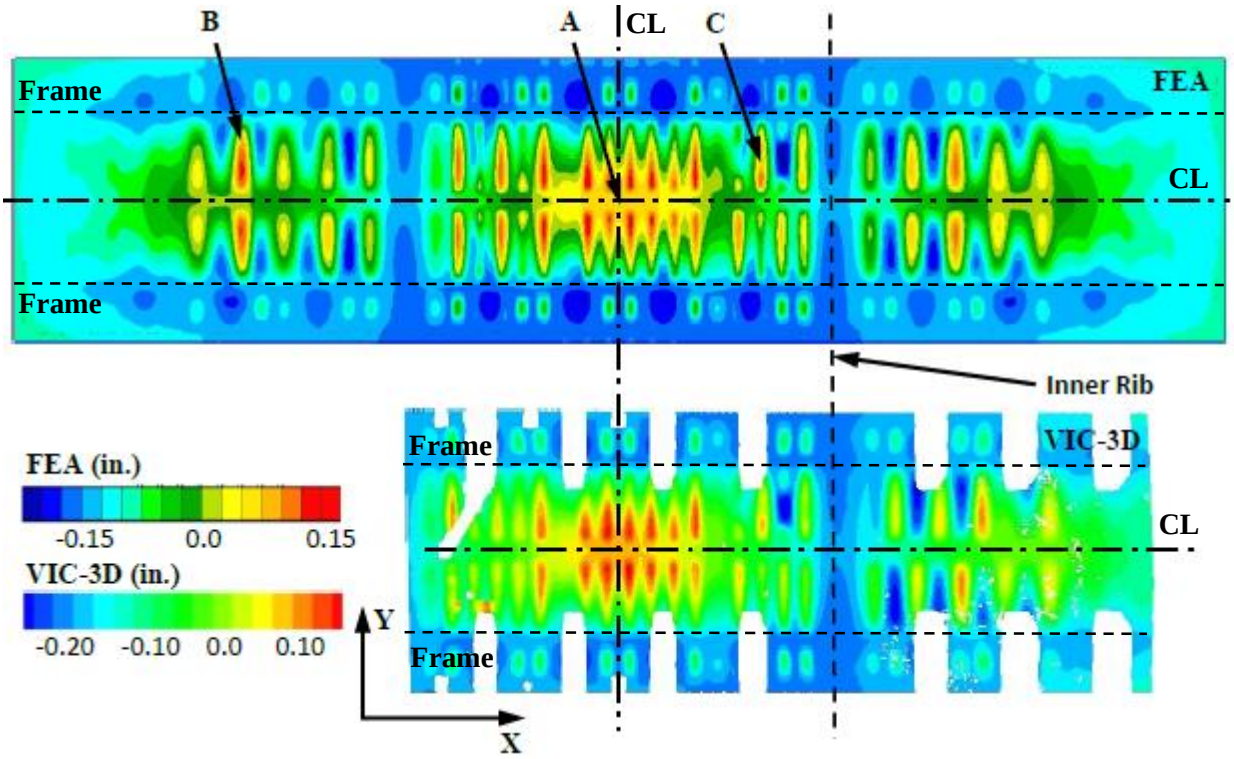

Figure 27. Out-of-plane deformation of the crown panel under 2.5-g + 1P DUL.

The crown panel strains at the mid-span top of the center frame (location A in Fig. 27) are shown in Fig. 28. The strain approached a moderately high compressive value of −0.0045 in./in. at the maximum test load of 2.5-g 165% DLL + 1P 150% DLL (262.4 kips actuator load). The strain displayed nearly linear characteristic over the entire load range. Upon closer examination, however, it can be seen that the slope of the strain versus load curve changes slightly at 238.5 kips actuator load (blue dashed line in Fig. 28), which corresponds to 2.5-g + 1P DUL. Above this load, only the mechanical component of the load is increased further, while the pressure load is kept constant (annotations in Fig. 28 through Fig. 30 highlight the two zones). The behavior observed in Fig. 28 is, therefore, indicative of the mechanical load being the primary driver of the frame response in the particular location considered. Good correlation between the test measurement and the FEA prediction is obtained (at the maximum load the FEA under-predicted the compressive strain by 8.7%).

The minimum principal skin strains in the proximity of the frame-stringer intersection located in a side section of the crown panel (location B in Fig. 27) are shown in Fig. 29. The strain at the maximum test load approaches a very high compressive value of −0.0070 in./in., i.e., approximately 0.0005 more negative that the same location under the 2.5-g 165% DLL only, as shown in Figure 23. The strain departs from the linear characteristic at approximately 75 kips actuator load. Considering very strong nonlinear behavior (at the maximum load strains obtained in the test and from the nonlinear analysis are almost double of those obtained from the linear analysis), a good comparison between the test measurement and the nonlinear FEA prediction is achieved (the FEA under-predicted the compressive strain by 11%).

The back-to-back skin strains in the center section of the crown panel (location C in Fig. 27) are shown in Fig. 30. Both tensile strains on the OML skin surface and compressive strains on the IML skin surface reach the absolute value of approximately 0.0040 in./in. at 2.5-g 165% DLL + 1P 150% DLL and match closely those obtained from the nonlinear FEA (the tensile strains are 5.0% under-predicted while the compressive strains are 6.1% over-predicted). Similar tensile and compressive strain magnitudes are indicative of this skin location response being strongly dominated by the bending strain component with almost non-existing in-plane strain participation, a condition

consistent with the buckled deformation shown in Fig. 27. The earlier-than-predicted initiation of the nonlinear behavior can be likely attributed to initial imperfections of the structure not reflected in the nominal FEM, especially since once the nonlinear response becomes fully developed the agreement between the test measurements and the nonlinear FEA results improves. Finally, the linear FEA produced substantially different results as small compressive strains were predicted on both OML and IML skin surfaces. These results imply that the linear FEA predicts a response comprising a small compressive in-plane strain component and a small bending strain component. Such a result is not surprising since the linear analysis is not capable of resolving large post-buckled deformations.

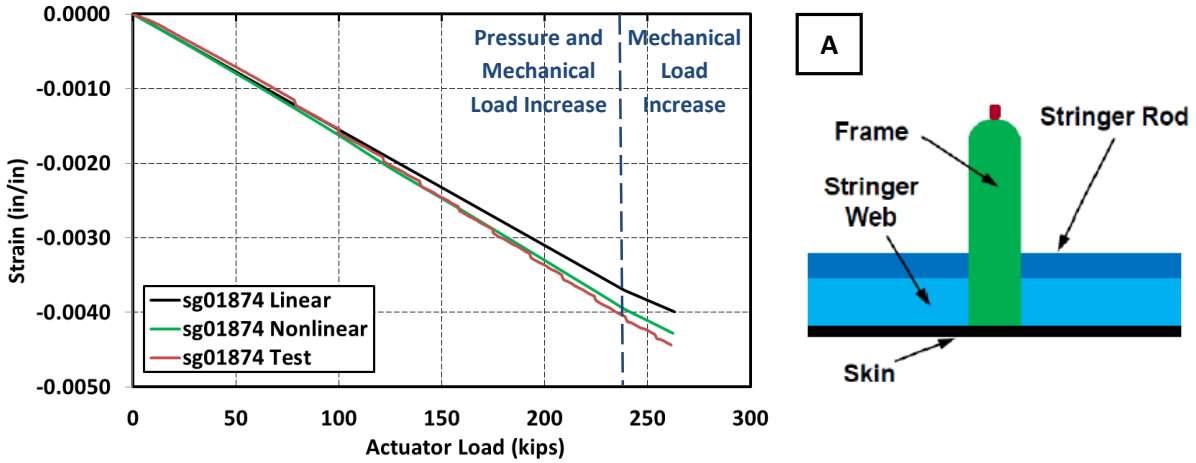

Figure 28. Strains at the top of the crown panel frame up to 2.5-g 165% DLL + 1P 150% DLL.

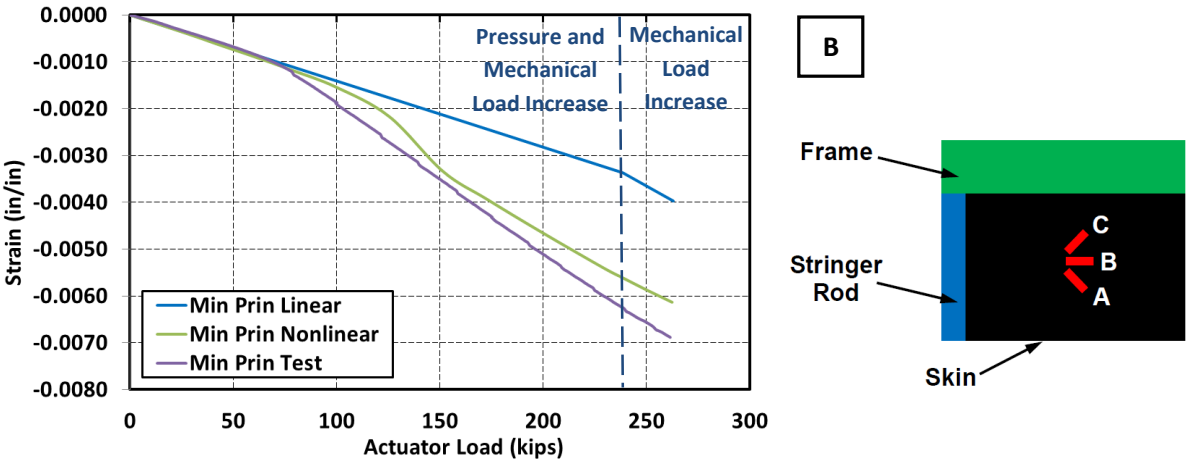

Figure 29. Minimum principal strains at the crown panel skin up to 2.5-g 165% DLL + 1P 150% DLL (sg01290A/sg01291B/sg01292C).

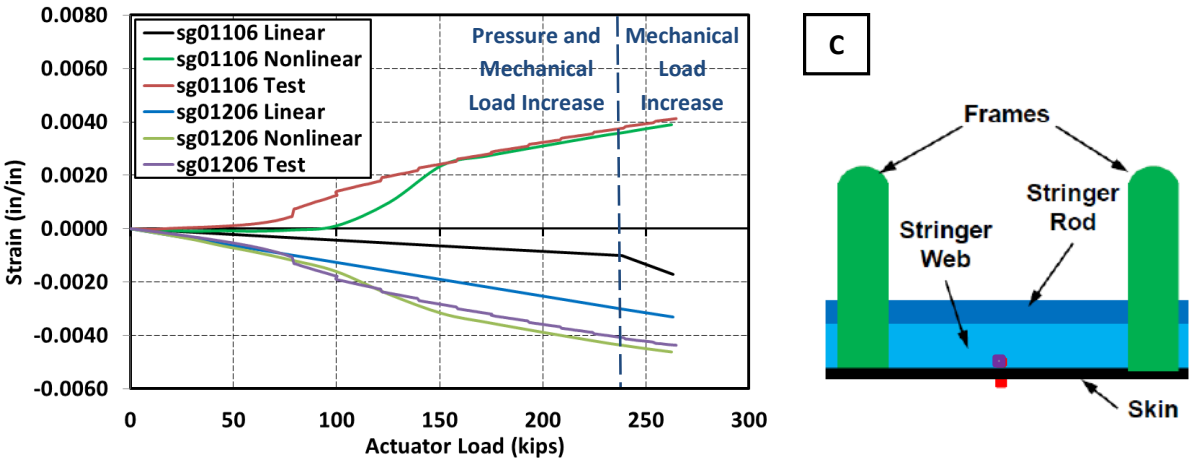

Figure 30. Crown panel skin back-to-back strains up to 2.5-g 165% DLL + 1P 150% DLL.

IV. Concluding Remarks

The FEA was used as the primary tool in designing the HWB test article and in guiding its test sequence and instrumentation. Due to computational expediency, the linear FEA analysis was conducted first and provided fairly accurate predictions for sizing of the test article substructure. Significantly more computationally intense nonlinear analysis was completed later and provided a higher fidelity insight into the mechanics of the HWB structure and filled in significant analysis gaps remaining due to the inherent limitations of the linear analysis. Furthermore, the nonlinear FEA permitted a design of test instrumentation that produced a more complete data set since the critical locations on the test article were precisely identified and appropriately instrumented.

The HWB center section proof-of-concept article was successfully tested under five loading scenarios up to DUL. For the two most critical load cases involving wing up-bending and wing up-bending with pressure, additional testing was conducted to 10% above DUL (or 165% DLL) for the wing up-bending load. The effort demonstrated the viability of the PRSEUS concept as the next generation airframe technology enabling non-conventional aircraft configurations and/or a weight-efficient approach to the design of conventional 'tube-and-wing' airframes. The predictive nonlinear FE analysis results compared very favorably with the test data and demonstrated that accounting for the geometrically nonlinear effects was required in the analysis. Specifically, two important behaviors that the linear FEA was unable to predict were identified by the nonlinear FEA. First, under pressure loads, the nonlinear FEA was able to accurately predict the suppression of the out-of-plane deformation rate due to the in-plane stretching. Second, under mechanical compressive loads, the nonlinear FEA accurately predicted extensive localized buckling of thin-skin bays and further post-buckled behavior. Understanding of this behavior is particularly important, as the PRSEUS design philosophy permits local buckling at low loads due to enhanced pull-out properties provided by the through-the-thickness reinforcement in the composite panels.

Successful completion of the sub-critical testing permitted the addition of the final test to failure with a severe discrete source damage, described in Part II of this paper.[30]

Acknowledgments

The authors acknowledge the entire team from The Boeing Company who built the test article and worked with the NASA Langley Research Center personnel in support of the testing activities. Contributions of Alex Velicki, Kim Linton, Krishna Hoffman, Patrick Thrash, Jaime Baraja, and Andy Harber from Boeing Research and Technology, Huntington Beach, CA are particularly acknowledged. Support of the testing effort by David Dawicke and Nathaniel Gardner (Analytical Services and Materials, Inc.) and Michael McNeil (Science and Technology Corporation) is also gratefully acknowledged.

References

[1]Li, V. and Velicki, A., "Advanced PRSEUS Structural Concept Design and Optimization," *Proceedings of the 12th AIAA/ISSMO Multidisciplinary Analysis and Optimization Conference*, AIAA-2008-5840, Victoria, BC, Canada, September 2008.

[2]Jegley, D. C., Velicki, A., and Hansen, D. A., "Structural Efficiency of Stitched Rod-Stiffened Composite Panels with Stiffener Crippling," *Proceedings of the 49th AIAA/ASME/ASCE/AHS/ASC Structures, Structural Dynamics and Materials Conference*, AIAA-2008-2170, Schaumburg, IL, April 2008.

[3]Velicki, A., Thrash, P. J., and Jegley, D. C., "Airframe Development for the Hybrid Wing Body Aircraft," *Proceedings of the 47th AIAA Aerospace Sciences Meeting Including The New Horizons Forum and Aerospace Exposition*, AIAA-2009-932, Orlando, FL, January 2009.

[4]Yovanof, N. P., Velicki A. and Li, V., "Advanced Structural Stability Analysis of a Nonlinear BWB-Shaped Vehicle," *Proceedings of the 50th AIAA/ASME/ASCE/AHS/ASC Structures, Structural Dynamics and Materials Conference*, AIAA-2009-2452, Palm Springs, CA, May 2009.

[5]Velicki, A. and Thrash, P. J., "Advanced Structural Concept Development Using Stitched Composites," *Proceedings of the 49th AIAA/ASME/ASCE/AHS/ASC Structures, Structural Dynamics and Materials Conference*, AIAA-2008-2329, Schaumburg, IL, April 2008.

[6]Thrash, P. J., "Manufacturing of a Stitched Resin Infused Fuselage Test Article," *Proceedings of The Composites and Advanced Materials Expo*, Orlando, FL, October 2014.

[7]Velicki, A., "Damage Arresting Composites for Shaped Vehicles – Phase I Final Report," NASA CR-2009-215932, NASA Langley Research Center, Hampton, VA, 2009.

[8]Lovejoy, A. E., Rouse, M., Linton, K. A., and Li, V.P., "Pressure Testing of a Minimum Gauge PRSEUS Panel," *Proceedings of the 52nd AIAA/ASME/ASCE/AHS/ASC Structures, Structural Dynamics and Materials Conference*, AIAA-2011-1813, Denver, CO, April 2011.

[9]Velicki, A., Yovanof, N. P., Baraja, J., Linton, K., Li, V., Hawley, A., Thrash, P., DeCoux, S., and Pickell, R., "Damage Arresting Composites for Shaped Vehicles – Phase II Final Report," NASA CR-2011-216880, NASA Langley Research Center, Hampton, VA, 2011.

[10]Velicki, A. and Jegley, D. C., "PRSEUS Development for the Hybrid Wing Body Aircraft," *Proceedings of the AIAA Centennial of Naval Aviation Forum "100 Years of Achievement and Progress,"* AIAA-2011-7025, Virginia Beach, VA, September 2011.

[11]Yovanof, N., Baraja, J, Lovejoy, A. E., and Gould, K. E., "Design, Analysis, and Testing of a PRSEUS Pressure Cube to Investigate Assembly Joints," *Proceedings of the 2012 Aircraft Airworthiness and Sustainment Conference*, TP5431, Baltimore, MD, April 2012.

[12]Yovanof, N. and Jegley, D. C., "Compressive Behavior of Frame-Stiffened Composite Panels," *52nd AIAA/ ASME/ASCE/AHS/ASC Structures Dynamics and Materials Conference*, AIAA-2011-1913, Denver, CO, April 2011.

[13]Przekop, A. and Jegley, D. C., "Testing and Analysis Validation of a Metallic Repair Applied to a PRSEUS Tension Panel," *Proceedings of the 54th AIAA/ASME/ASCE/AHS/ASC Structures, Structural Dynamics and Materials Conference*, AIAA-2013-1735, Boston, MA, April 2013.

[14]Jegley, D. C. and Velicki, A., "Status of Advanced Stitched Unitized Composite Aircraft Structure," *Proceedings of the 51st AIAA Aerospace Sciences Meeting*, AIAA 2013-0410, Grapevine, TX, January 2013.

[15]Velicki, A. and Thrash, P. J., "Damage Arrest Design Approach Using Stitched Composites," *The Aeronautical Journal*, Vol. 115, No. 1174, pp. 789-795, Royal Aeronautical Society, London, UK, December 2011.

[16]Bergan, A., Bakuckas, J., Lovejoy, A. E., Jegley, D. C., Linton, K., Korkosz, G., Awerbuch, J., and Tan, T., "Full-Scale Test and Analysis of a PRSEUS Fuselage Panel to Assess Damage-Containment Features," *Proceedings of the 2011 Aircraft Airworthiness and Sustainment Conference*, TP4558, San Diego, CA, April 2011.

[17]Velicki, A. and Thrash P. J., "Blended Wing Body Structural Concept Development," *Proceedings of Aircraft Structural Design Conference*, Liverpool, UK, October 2008.

[18]Ambur, D. A., Rouse, M., Starnes, J. H., and Stuart, M. J., "Facilities for Combined Loads Testing of Aircraft Structures to Satisfy Structural Technology Development Requirements," *Proceedings of the 5th Annual Advanced Composites Technology Conference*, Seattle, WA, August 1994.

[19]Wu, H. T., Shaw, P., and Przekop, A., "Analysis of a Hybrid Wing Body Center Section Test Article," *Proceedings of the 54th AIAA/ASME/ASCE/AHS/ASC Structures, Structural Dynamics and Materials Conference*, AIAA-2013-1734, Boston, MA, April 2013.

[20]Przekop, A., Wu, H. T., and Shaw, P., "Nonlinear Finite Element Analysis of a Composite Non-Cylindrical Pressurized Aircraft Fuselage Structure," *Proceedings of the 55th AIAA/ASME/ASCE/AHS/ASC Structures, Structural Dynamics and Materials Conference*, AIAA-2014-1064, National Harbor, MD, January 2014.

[21]Przekop, A., Jegley, D. C., Rouse, M., and Lovejoy, A. E., "Finite Element Analysis and Test Results Comparison for the Hybrid Wing Body Center Section Test Article," NASA TM-2016-218973, NASA Langley Research Center, Hampton, VA, 2016.

[22]MSC Nastran 2012.2 Quick Reference Guide, MSC Software Corporation, Santa Ana, CA, 2012.

[23]Title 14 Code of Federal Regulation, Part 25 "Airworthiness Standards: Transport Category Airplanes," Subpart C "Structure," Electronic Code of Federal Regulations, http://www.ecfr.gov/cgi-bin/text-idx?c=ecfr&tpl=/ecfrbrowse/Title14/14cfr25_main_02.tpl

[24]Jegley, D. C., Przekop, A., Rouse, M., Lovejoy, A. E., Velicki, A., Linton, K., Wu, H. T., Baraja, J., Thrash, P. J., and Hoffman, K., "Development of Stitched Composite Structure for Advanced Aircraft," *Proceedings of the American Society for Composites 30th Technical Conference*, Paper 1840, East Lansing, MI, September 2015.

[25]Jegley, D. C., Rouse, M., Przekop, A., and Lovejoy, A. E., "The Behavior of a Stitched Composite Large-Scale Multi-Bay Pressure Box," NASA TM-2016-218972, NASA Langley Research Center, Hampton, VA, 2016.

[26]McGowan, D. M., Ambur, D. R., and McNeil, S. R., "Full-field Structural Response of Composite Structures: Analysis and Experiment," *Proceedings of the 44th AIAA/ASME/ASCE/AHS/ASC Structures, Structural Dynamics and Materials Conference*, AIAA 2003-1623, Norfolk, VA, April 2003.

[27]Moore, J. P., Przekop, A., Juarez, P. D., and Roth, M. C., "Fiber Optic Rosette Strain Gauge Development and Application on a Large-Scale Composite Structure," NASA TM-2016-218970, NASA Langley Research Center, Hampton, VA, 2016.

[28]Horne, M. R. and Madaras, E. "Evaluation of Acoustic Emission SHM of PRSEUS Multi-Bay Box Tests," NASA TM-2016-218976, NASA Langley Research Center, Hampton, VA, 2016.

[29]Johnston, P. H. and Juarez, P. D., "Nondestructive Evaluation of PRSEUS During Large-Scale Load Testing and Rod Push-Out Testing," NASA TM-2016-218978, NASA Langley Research Center, Hampton, VA, 2016.

[30]Przekop, A., Jegley, D. C., Lovejoy, A. E., Rouse, M., and Wu, H. T., "Testing and Analysis of a Composite Non-Cylindrical Aircraft Fuselage Structure, Part II: Severe Damage," *Proceedings of the 57th AIAA/ASME/ASCE/AHS/ASC Structures, Structural Dynamics and Materials Conference*, AIAA-2016-2177, San Diego, CA, January 2016.